Computational Science and Engineering
(International Master's Program)

Technische Universität München

Master's Thesis in
Computational Science And Engineering

Courant-Friedrichs-Lewy Type Conditions For Approximating Quantum Dynamics On A Digital Quantum Computer

Rahul Banerjee

Computational Science and Engineering
(International Master's Program)

Technische Universität München

Master's Thesis in
Computational Science And Engineering

Courant-Friedrichs-Lewy Type Conditions For Approximating Quantum Dynamics On A Digital Quantum Computer

Author:	Rahul Banerjee
1st examiner:	Univ.-Prof. Dr. Christian Mendl
Submission Date:	April 1, 2022

I hereby declare that this thesis is entirely the result of my own work except where otherwise indicated. I have only used the resources given in the list of references.

April 1, 2022 Rahul Banerjee

Acknowledgments

First and Foremost, I would like to thank Professor Christian Mendl for his constant guidance, inputs and support throughout the duration of this thesis and all the preceding foundation work, part of which was done during a pandemic phase that turned out to be quite difficult from a personal perspective. I would also like to thank my parents who despite being thousands of miles away, have always motivated and supported me in all my endeavours. And last but certainly not the least, I would like to thank my friends who were a constant source of strength throughout my Master's journey.

"In order to seek truth, it is necessary once in the course of our life to doubt, as far as possible, of all things."

-René Descartes

Abstract

In time integration of hyperbolic partial differential equations (PDEs), the Courant-Friedrichs-Lewy (CFL) Criterion puts restrictions on the time-step size used in some simulation schemes and it becomes necessary to adhere to that in order to obtain a physically viable solution that obeys locality. In a similar manner, while evaluating the dynamics of a quantum mechanical system via the time dependent Schroedinger's equation or via Heisenberg's equation, it is necessary to establish a similar criterion to ensure that locality is obeyed. This is also required as Special Relativity limits the spatial spread of information in a time step and any theory that obeys locality is bound by this. The aim of this thesis is to investigate a suitable criterion (Lieb-Robinson bounds) and find good estimates for it using numerical simulations and also discuss how this criterion can impact the efficiency of a digital quantum computer, in terms of the number of quantum logic gates used.

Contents

Part I.

Motivation And Scope

1. Motivation

Physics, as it stands today, explains the laws of nature in terms of interactions between bodies at different scales. The interactions are :

- Gravity
- Electromagnetic
- Strong
- Weak

Aside from Gravity, which is explained by the General Theory of Relativity, all the other fundamental interactions are explained by the Standard Model, which is based on Quantum Field Theory, which in turn rests on the foundational principles of Quantum Mechanics.

Quantum Mechanics provides us with a complete mathematical description of interactions at the atomic and subatomic levels. Central to this description are the ideas of **Wave Functions** and **Operators**. The Wave Function, typically represented by ψ, is a complete description of the quantum state of a body and **Operators** are the properties of the body that one is typically interested in measuring. These properties may include Energy, Momentum, Position etc.

Although quantum mechanics in general, has little in common with how classical mechanics is formulated, there are certain factors that unify both the domains when dealing with systems that obey the **Principle of Locality**. The locality principle states that : in a physical system governed by natural laws, a point is only affected by events that occur in its immediate surroundings. Locality is built into the laws of classical field theories such as the Theory of Relativity and forms an inviolable principle in its treatment of the spacetime manifold and causality.

The status of quantum mechanics, especially regarding its ontology, is one of the most baffling questions in physics and there are several schools of thought regarding it. Thought experiments such as the famous **Einstein-Podolsky-Rosen (EPR)** experiments [10], seems to suggest that quantum mechanics violate the principle of locality but subsequent, careful analysis has concluded that although quantum mechanics exhibits traits that does not coincide with **local realism**, it certainly is local from the perspective of Special Relativity, in

that there is no faster-than-light transfer of information is possible and information transfer is bounded by certain speeds.

The case for classical systems is simpler. They are all derived as consequences of the General Theory of Relativity and are always local. When simulating certain physical systems, such as waves, it becomes important to consider this idea of locality to get meaningful, convergent solutions. Such criteria can be obtained by a mathematical treatment of the numerical methods used to simulate the phenomenon in question.

Quantum mechanical principles are utilized today in the design of digital quantum computers. An ideal, universal digital quantum computer has the ability to simulate quantum process using resources that are orders of magnitude less than what would otherwise be needed to simulate those systems on classical computers. Having said that, we still do not have such devices today and we are currently in the era of **Noisy Intermediate-Scale Quantum (NISQ)** computers that are extremely noisy in nature and prone to large errors if used for sustained time-periods. While simulating a quantum many-body system in such devices, it is advisable to set up the circuit using as few quantum logic gates as possible, to minimize sources of error. Following the principle of locality, if we can estimate the distance to which quantum information can spread over a single time-step during the simulation, it is then possible to treat spatially distant areas of the circuit independently of each other, thereby reducing the need to cross-connect a large number of noisy qubits, resulting in the usage of fewer quantum logic gates [25]. Thus, estimating the speed at which quantum information spreads within a system assumes significant importance in the design of efficient and accurate digital quantum computers, especially in the NISQ era.

2. Scope

In this thesis, we examine the dynamical behaviour of a system, called the **Transverse Field Ising Model (TFIM)**, which is a well studied case in the dynamics of quantum many-body systems. Good references exist that are used as benchmarks for our simulations.

We first study the dynamical response of the TFIM to a local perturbation using a **Time-Ordered Correlation Function** [6], that measures how the quantum information generated from an initial perturbation spreads across the system over time, a process known as **Relaxation**. The correlation function is then used to estimate the speed of this relaxation process, quantified by the **Lieb-Robinson Velocity**, v_{LR}. We then compare our estimation with existing results [26] to see if our approach obtains a better estimate of the v_{LR}.

Finally, we discuss how the better estimation of the v_{LR} can be utilized to design more efficient circuits on a digital quantum computer by utilizing fewer logic gates in the circuit design [25] [14] and what are the existing challenges and limitations of our approach.

Part II.

Introduction and Background Theory

3. Quantum Mechanics Primer

Central to our understanding of the systems discussed in this work, and to the general nature of the problem types in this domain, lie the principles and the mathematical framework of Quantum Mechanics. We briefly discuss the most essential ideas from this theory. The postulates that form the core of quantum mechanics can be found in A.1. The terminology and derivations are largely inspired from Nielsen and Chuang[24].

3.1. States and Operators

3.1.1. States

States in quantum mechanics are simply vectors in some **Hilbert Space,** $\mathcal{H}$, that is endowed with a set of **Linearly Independent, Orthonormal** set of **Basis Vectors**. The system which we will be most concerned with, is the **Qubit**. A Qubit is defined as a vector in a two-dimensional state space, with the basis vectors being $|0\rangle$ **and** $|1\rangle$. An arbitrary state in this space is written as

$$|\psi\rangle = \alpha\,|0\rangle + \beta\,|1\rangle \tag{3.1}$$

with the **Normalization Condition** constraining $\alpha, \beta \in \mathbb{C}$ as

$$\alpha^2 + \beta^2 = 1 \tag{3.2}$$

3.1.2. Operators

Measurable quantities, such as Energy, Momentum, Position etc in quantum mechanics are all represented by operators. Given a set of basis vectors, an operator can be simply though of as a matrix, that acts on an input state vector to produce an output state vector. If an operator O, acts on an input state $|\psi\rangle$ and outputs a state $|\psi'\rangle$, it can be briefly written as

$$O\,|\psi\rangle = \left|\psi'\right\rangle \tag{3.3}$$

Operators that correspond to measurable quantities in quantum mechanics, called observables, have some special properties. For an operator O, the properties can be summarized can be summarized as

Linearity

For a linear combination of 2 state vectors, $\alpha |\Psi\rangle + \beta |\Phi\rangle$, the action of the operator O is linear over its arguments.

$$O(\alpha |\Psi\rangle + \beta |\Phi\rangle) = O(\alpha |\Psi\rangle) + O(\beta |\Phi\rangle) \tag{3.4}$$

Self-Adjoint

For a linear operator O, being self-adjoint refers to the fact that the operator is equal to its own **conjugate-transpose**.

$$O = O^{\dagger} \tag{3.5}$$

When these two properties are combined, the resulting operator is said to be **Hermitian**. Hermitian operators have real eigenvalues and these eigenvalues correspond to measurement outcomes of the corresponding observable.

The **Time Independent Schrödinger Equation** is used to estimate the **Stationary States** of a quantum system that is subjected to the action of some operator. For example, if an energy hamiltonian $\hat{H}$ acts on some system, whose wave function is given by $|\Psi\rangle$, then the The Time Independent Schrödinger Equation is written as

$$\hat{H} |\Psi\rangle = E |\Psi\rangle \tag{3.6}$$

This is an eigenvalue equation where the real-valued quantity E corresponds to the energy eigenvalues of the system at any given time and the $|\Psi\rangle$ represents the corresponding eigenstates.

3.2. Time Evolution of Quantum Systems

3.2.1. Schrödinger Picture

If the states of a closed quantum system are dependent on time, then the time-evolution of the system is captured by a linear, first-order differential equation

$$i\hbar \frac{d|\psi\rangle}{dt} = H|\psi\rangle \tag{3.7}$$

This is the Time Dependent Schrödinger Equation and its solution at different times give us

the time-evolution of the closed quantum system. If the Hamiltonian H is time-independent, then the equation can be solved as

$$|\Psi(t)\rangle = e^{-i\hat{H}t/\hbar}|\Psi(0)\rangle \tag{3.8}$$

where, $|\Psi(0)\rangle$ is the initial state and $|\Psi(t)\rangle$ is the state after time t. The term $e^{-i\hat{H}t/\hbar}$ is the time-evolution operator and can be written succinctly as $\hat{U}$. Using this notation, the time evolution can be written as

$$|\Psi(t)\rangle = \hat{U}|\Psi(0)\rangle \tag{3.9}$$

If w
e compare this with Equation 3.3, we can see that $\hat{U}$ is an operator. In fact, it is a **Unitary Operator** and is responsible for the temporal dynamics of a quantum system.

Unitary operators are **Norm-Preserving**, which means that the length of the vectors, before and after the action of the unitary operator, remains the same. Mathematically, for some Hilbert Space H, equipped with an inner-product $\langle , \rangle$ and two vectors x and y

$$\langle Ux, Uy\rangle_H = \langle x, y\rangle_H \tag{3.10}$$

3.2.2. Heisenberg Picture

The Time Dependent Schrödinger Equation defines the time-evolution of a quantum state that is under the influence of quantum dynamics, encapsulated in the unitary time-evolution operator $\hat{U}$. In this approach, the observable is assumed to be fixed and the quantum state is assumed to have a time-dependency. In an alternative approach, known as the Heisenberg approach, the reverse is assumed to be true, i.e the state is assumed to be fixed but the observable is now considered to have a time dependency. To develop the governing equations in this picture, we start by considering an arbitrary Hermitian operator B and computing its expectation values :

$$\begin{aligned}\langle B\rangle &= \langle\psi(t)|B|\psi(t)\rangle \\ &= \left\langle e^{-iHt/\hbar}\psi(0)|B|e^{-iHt/\hbar}\psi(0)\right\rangle \\ &= \left\langle \psi(0)\left|e^{iHt/\hbar}Be^{-iHt/\hbar}\right|\psi(0)\right\rangle\end{aligned} \tag{3.11}$$

Now, the term $e^{iHt/\hbar}Be^{-iHt/\hbar}$ can be considered in its entirety as the time evolution of the observable B, thus giving us the expression :

$$B(t) = e^{iHt/\hbar}Be^{-iHt/\hbar} \tag{3.12}$$

We can formulate the Heisenberg equation of motion by considering the time derivative of the operator.

$$\begin{aligned}\frac{d}{dt}B(t) &= \frac{iH}{\hbar}e^{iHt/\hbar}Be^{-iHt/\hbar} - e^{iHt/\hbar}B\frac{iH}{\hbar}e^{-iHt/\hbar} \\ &= \frac{i}{\hbar}e^{iHt/\hbar}[H,B]e^{-iHt/\hbar} = \frac{i}{\hbar}[H,B(t)]\end{aligned} \tag{3.13}$$

Thus, the time derivative of an observable is governed by its commutator with the system Hamiltonian.

3.3. Transverse Field Ising Model

The Transverse Field Ising Model (TFIM) is an example of a quantum many-body system that consists of a lattice-graph arrangement of Spin-1/2 particles, mostly Fermions such as electrons, that repeat periodically in all spatial directions **(Periodic Boundary Conditions)**. An indicative sketch is provided in Figure 3.1 There are two kinds of interactions that are taken into considerations in such systems.

- Nearest neighbor interactions between lattice sites ***i*** and ***j*** whose strength is set by a constant J_{ij} having the units of energy.
- Interaction of each lattice site with an external magnetic field that acts perpendicular to the lattice plane. The relative strength of the external field compared to the nearest neighbour interaction is given by a coupling coefficient h_j.

Mathematically, the Hamiltonian of such a system is written as:

$$H(\sigma) = \sum_{\langle i,j\rangle} -J_{ij}\sigma_i\sigma_j - \sum_j h_j\sigma_j \tag{3.14}$$

Here, the σ_i represents the spin operator, typically Pauli Matrices, acting on a specific lattice site. Each spin configuration of the lattice is associated with an energy and the probability that the system exists in a specific specific spin configuration at a given temperature is governed by the **Boltzmann Distribution**:

$$P_\beta(\sigma) = \frac{e^{-\beta H(\sigma)}}{Z_\beta} \tag{3.15}$$

where $\beta = (k_B T)^{-1}$, k_B being the **Boltzmann Constant** and the normalization constant $Z_\beta = \sum_\sigma e^{-\beta H(\sigma)}$ is called the **Partition Function**
In the form used in (3.14), the sign of the term J_{ij} can be used to classify nearest-neighbor interactions into the following cases:

- $J_{ij} > 0$: Ferromagnetic Interaction.
- $J_{ij} < 0$: Antiferromagnetic Interaction
- $J_{ij} = 0$: No Interaction..

The sign of the term h_j can be used to classify individual spin sites into the following cases:

- $h_j > 0$: Site j wants to line up along the direction of the external field.
- $h_j < 0$: Site j wants to line up against the direction of the external field.
- $h_j = 0$: No influence on the site.

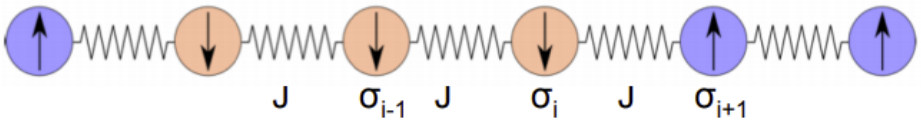

Figure 3.1.: 1-Dimensional Transverse Field Ising Model. Image Courtesy: Paolo Molignini

4. Hyperbolic Partial Differential Equations (PDEs)

4.1. Formulation

For our case, we confine ourselves to the analysis of PDEs that are first order in both time and space. In other words, our PDEs consist of only the first order time and space derivatives of the quantities of interest. The general form of PDEs of first order with n variables is:

$$F\left(x_1, \ldots, x_n, u, u_{x_1}, \ldots u_{x_n}\right) = 0 \tag{4.1}$$

where x_i is an independent variable, u_i is some quantity whose evolution we would like to study and u_{x_i} is the first order derivative of the variable u_i w.r.t x_i, or, $u_{x_i} = \partial u_i / \partial x_i$. In general, $u_i = f(x_1, x_2, ..., x_n)$
When dealing with PDEs of the first order, hyperbolic PDEs have wave-like formulations that obey the following general form:
Consider some quantity u to be dependant on time t and space x or $u = u(x, t)$ and another constant quantity a, defined as the wave speed. Then, **well-posed** hyperbolic PDE of the first order, together with an **initial condition** looks like:

$$u_t + a u_x = 0, \quad x \in \mathbb{R}, t > 0 \tag{4.2}$$

$$u(x, 0) = g(x) \tag{4.3}$$

where g is a compactly supported smooth function.

Equation 4.3 is an example of an **Initial Value Problem (IVP)** because it encapsulates the system behaviour by specifying both the initial state and the governing law. For an IVP to be considered **well-posed**, the following conditions must hold:

- A solution exists.
- The solution is unique.
- The solution depends on the data in a continuous manner.

For the problems that we will consider, the above criteria are always satisfied.

4.2. Solutions and Properties

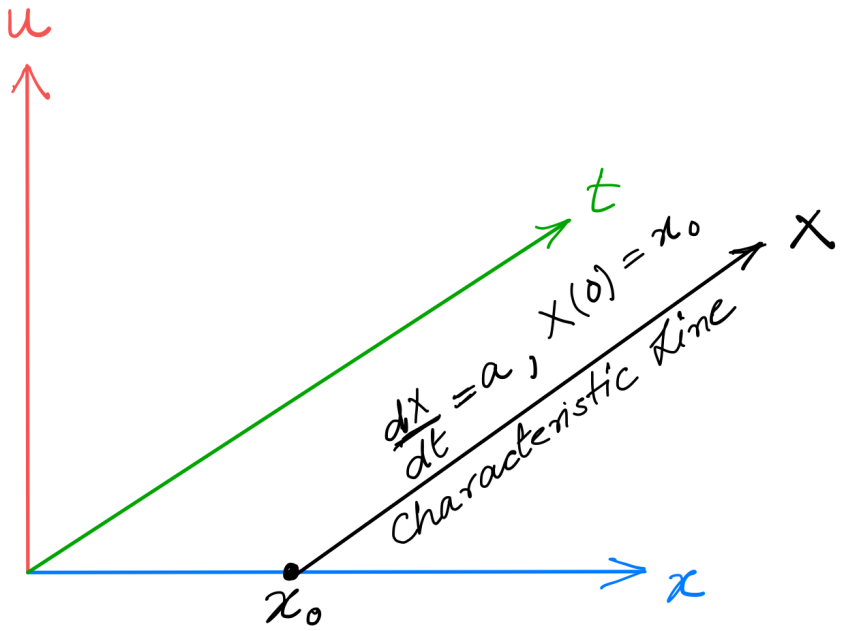

Figure 4.1.: Characteristic Curves given by $\frac{dX}{dt} = a$

We maintain the symbol convention introduced in the previous section and further define **characteristics X** as the curves in the (x, t) plane, that are solutions to the Ordinary Differential Equation (ODE) given by (see Fig 4.1):

$$\frac{dX}{dt} = a, \quad X(0) = x_0 \tag{4.4}$$

We than have that,

$$u(X(t), t) = g(x_0) \tag{4.5}$$

In other words, the solutions remain constant along the characteristic curves. If we can generate characteristic curves for each point on the x-axis, the entire solution can be computed.

Further, since $\frac{d}{dt}u(X(t), t) = 0$ by chain rule and $u(X(0), 0) = g(x_0)$, we get:

$$u(x, t) = g(x - at) \tag{4.6}$$

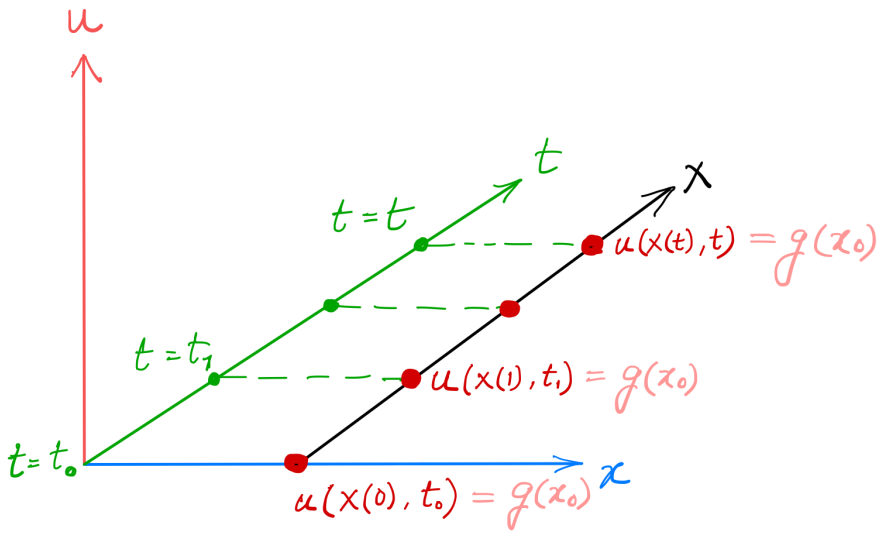

Figure 4.2.: Solution along Characteristic Curves given by $u(x,t) = g(x - at)$

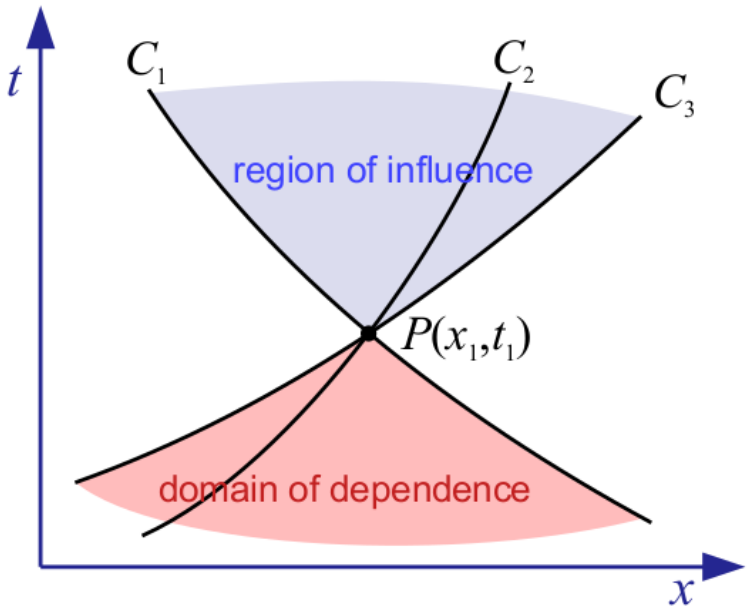

Figure 4.3.: Domain of influence and dependence of a point $P(x_1, t_1)$

See Fig 4.2.

In this formulation, the solution along a particular characteristic curve only depends on the solution along that line at $t = 0$ and not on the initial values at any other site. Thus, disturbances at some location along x cannot spread to any other location if the characteristic curves are parallel to one another. In a more general setting, the characteristic curves may intersect at some point and information along the different characteristic curves may flow at different propagation speeds. Then the solution domain looks somewhat like this:

In Fig 4.3, the characteristic curves C_1, C_2, C_3 intersect at the point $P(x_1, t_1)$ and forms 2 distinct regions. The **domain of dependence** consists of all the points in the past that have an influence on the point in question. The **region of influence** consists of all the points in the future that can be influenced by the point in question. The domains have a unique 'light-cone' like causal structure and are bounded by characteristics with the largest and smallest propagation speeds.

4.3. Linear Advection Equation and the Courant-Friedrichs-Lewy condition

An example of a hyperbolic PDE is the **1D Linear Advection Equation**, which models the dift of an incompressible fluid. The quantity of interest, $u(x, t)$ represents the particle density and it only changes due to convective processes. The equation is:

$$\frac{\partial u}{\partial t} + c\frac{\partial u}{\partial x} = 0 \tag{4.7}$$

Here, $u = u(x, t), x \in \mathbb{R}$ and c is a non-zero velocity, assumed constant for simplicity. The unique solution is determined by the initial condition $u_0 := u(x, 0)$ and is given by $u(x, t) = u_0(x - ct)$.

For our purposes, we solve the 1D advection equation numerically using the **Lax-Wendroff Method** [19], which is an explicit method, second-order accurate in both time and spatial discretization. The exact derivation of the scheme is elaborated in the Methods section of this document. The important thing to remember at this stage is the fact that while utilizing finite-difference schemes for hyperbolic PDEs, special care has to be taken while choosing the resolution for space and time discretization. This is to ensure that the **numerical domain of dependence**, obtained from the method, respects the **analytical domain of dependence**, introduced in the previous section. Only then, a physically accurate solution can be obtained.

Intuitively, in the numerical scheme we try to measure the amplitude of a propagation

at different time-steps. If the propagation has a speed v and the spatial grid has a size Δx, then after one time-step of duration Δt, a point should travel a distance of $v\Delta t$ at most and the spatial grid should have a resolution that is greater than or equal to this value, otherwise it would appear that the propagation *jumps* over certain points and reaches the next point which is something non-physical. Briefly $v\Delta t \leq \Delta x$. This is known as the **Courant–Friedrichs–Lewy condition** [9].

5. Relaxation, Thermalization and the flow of Quantum Information

5.1. Scrambling and Thermalization in Quantum Systems

In the study of quantum many-body systems, quantities called **Dynamical Correlations** play an important role and provide information about the nature of excitations in such systems [11]. When a quantum many-body system is perturbed locally, the dynamical response of the system, known as **Relaxation**, is quantified using **Time Ordered Correlation Functions**. Such quantities indicate how information from the perturbation spreads through the system over time. Another related process in the study of such systems is that of **Thermalization**, which refers to the time evolution of the observables till they approach equilibrium.

The phenomenon of scrambling is governed by physical laws that exhibit a linear, light-cone like behaviour, very similar to the causal light cones observed in special relativity. Thermalization is governed by laws that resemble hydrodynamic diffusion and it takes place over very long time-scales as compared to relaxation [14]. For our purposes, we focus exclusively on scrambling and develop a numerical scheme to measure dynamic correlations and estimate the rate at which they spread across the system.

In general, time-ordered dynamical correlation functions are of the form $\langle W(t)V(0)\rangle$, that describes the **relaxation** of a many-body system following an initial perturbation by an operator V that is then tested at a later time using the operator W.

Typically, a time-ordered correlation function $C_{i-j}(t)$ can be defined in the following manner

$$\begin{aligned} C_{i-j}(t) &= \langle W_i(t)V_j(0)\rangle \\ &= \langle\psi(0)|W_i(t)V_j(0)|\psi(0)\rangle \\ &= \langle\psi(0)|e^{iHt}W_i(0)e^{-iHt}V_j(0)|\psi(0)\rangle \\ &= \langle\psi(0)|U^{+}W_i(0)UV_j(0)|\psi(0)\rangle \end{aligned} \tag{5.1}$$

Here, $|i-j|$ is the distance between a given lattice site and the site where the initial perturbation is applied, $U = e^{-iHt}$ is the time-evolution operator and W_d is the unitary operator

acting locally at a site. In this approach, we deal with the Heisenberg picture of time-evolution as we time evolve the operator W_d in a unitary fashion.

5.2. Lieb-Robinson Bounds

Lieb-Robinson bound is a theoretical upper bound that quantifies the speed at which information can spread within closed, translation-invariant and non-relativistic quantum systems. Although this bound is not derived from the postulates of special relativity, its existence nevertheless reinforces the idea that information cannot travel instantaneously or *superluminally* in quantum systems. Further, the bound has many similarities with the concept of the finite group velocity in classical wave propagation.

In their original work [20], the authors estimated the bounds on an n-dimensional lattice and stated it as follows :

Theorem 1 *In a translation invariant quantum system, for any observables A and B with finite supports X and Y, respectively, in the system, and for any time $t \in \mathbb{R}$, the following holds for some positive constants a, c, v:*

$$||[A(t), B]|| \leq ce^{-a(d(X,Y)-v|t|)} \tag{5.2}$$

Here, $d(X, Y)$ is the distance between the sets X and Y and $[A, B]$ is the usual commutator. The positive constant v only depends on the nature of interaction between the sets X and Y and the lattice structure. It is called the **Lieb-Robinson Velocity**. The expression above further shows that for times $|t| < d(X, Y)/v$, the quantity on the right-hand side becomes exponentially small which implies that outside the light-cone that is defined by the Lieb-Robinson velocity, the quantity $||[A(t), B]||$ decays exponentially.

It is to be noted that the bound has nothing to do with the actual quantum state of the system but is determined by the Hamiltonian that governs the system. The bound has important implications in several domains, including quantum computing. Two regions of the same system, separated in space, can be treated as two independent sub-systems with no cross effects on each other. This has the potential of simplifying many numerically intensive calculations.

5.3. Lieb-Robinson Bounds and Digital Quantum Computers

The existence of the Lieb-Robinson bounds has important implications in the domain of gate-based quantum computing, especially for problems that involve the time-evolution of a Hamiltonian. We consider the approach used in [14] to utilize the Lieb-Robinson bounds to break the time-evolution unitary corresponding to the full Hamiltonian H, into

smaller unitaries that perform time-evolution for a smaller part of the Hamiltonian, and by extension, of the circuit itself. The overall idea is visualized in Figure 5.1. In the figure, time goes downwards and each rectangular block represents some time-evolution unitary U.

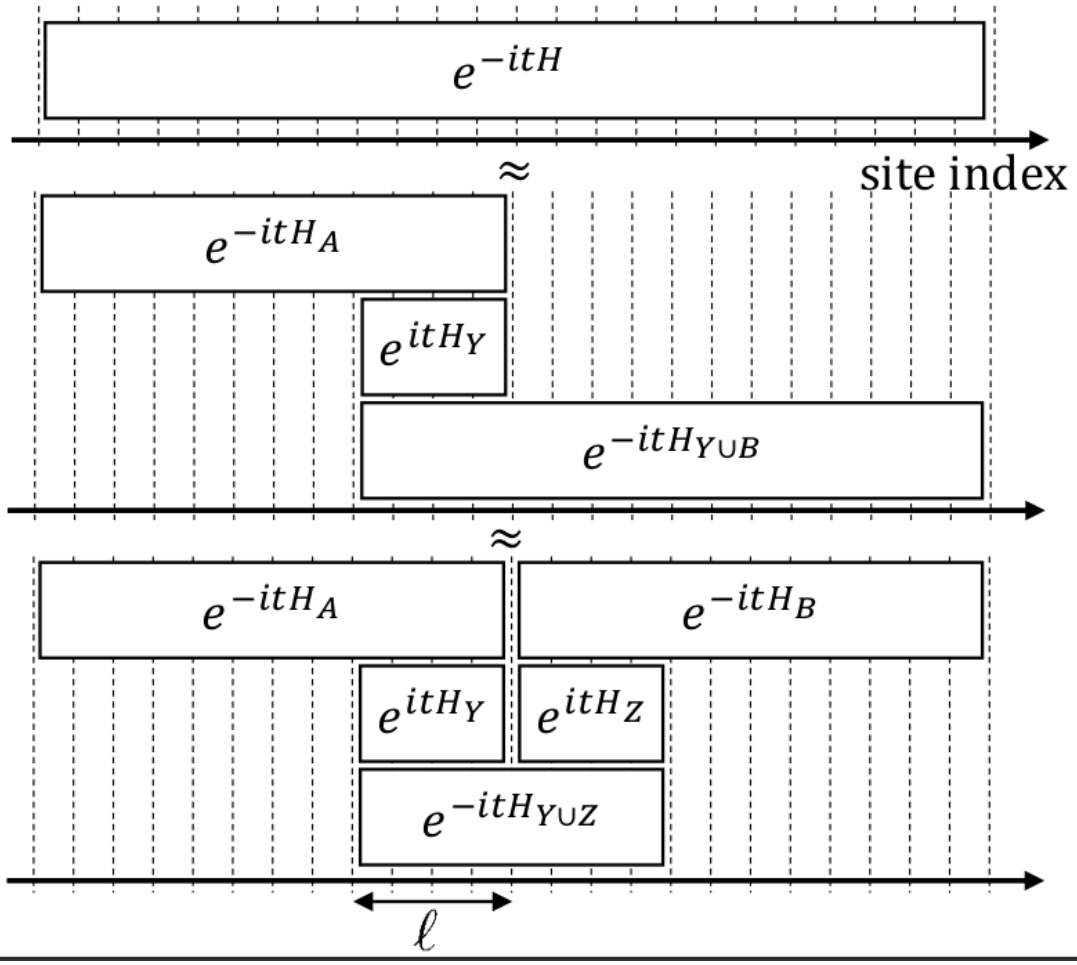

Figure 5.1.: Dividing the overall unitary into smaller parts. Figure adapted from [14].

Theorem 2 *Let $H(t) = \sum_{X\subset\Lambda} h_X(t)$ be a time-dependent Hamiltonian on a lattice Λ of n qubits, embedded in the Euclidean metric space $\mathbb{R}^D$. Assume that every unit ball contains O(1) qubits and $h_X = 0$ if $diam(X) > 1$. Also assume that every local term $h_X(t)$ is efficiently computable (e.g., analytic), piecewise slowly varying on time domain [0, T], and has $||h_X(t)|| \leq 1$ for any X and t. Then, there exists a quantum algorithm that can approximate the time evolution of H for time T to accuracy ϵ using $O(Tnpolylog(Tn/\epsilon))$ 2-qubit local gates, and has depth $O(Tpolylog(Tn/\epsilon))$.*

The key insight from Theorem 2 is that the full time-evolution operator $U = e^{-iHt}$ can be

written as an approximate product.

$$e^{-itH} \approx \left(e^{-itH_A}\right)\left(e^{+itH_Y}\right)\left(e^{-itH_{Y\cup B}}\right) \tag{5.3}$$

Here, $A = \Lambda$ and in general, A and B can be large regions but Y is a small subset of A. As long as Y is large enough, the error in the approximation is exponentially small. This can be further written as:

$$e^{-itH_{Y\cup B}} \approx \left(e^{-itH_B}\right)\left(e^{+itH_Z}\right)\left(e^{-itH_{Y\cup Z}}\right) \tag{5.4}$$

Leading to the total unitary being expressed as:

$$e^{-itH} \approx \left(e^{-itH_A}\right)\left(e^{+itH_Y}\right)\left(e^{-itH_{Y\cup B}}\right) \quad = \left(e^{-itH_A}\right)\left(e^{+itH_Y}\right)\left(e^{-itH_B}\right)\left(e^{+itH_Z}\right)\left(e^{-itH_{Y\cup Z}}\right) \tag{5.5}$$

This general idea can be used iteratively to split down the total system into smaller parts and then evolving each of the smaller parts individually using known algorithms. How small the parts are allowed to be is determined by the Lieb-Robinson bounds for the system in question. The authors express this as a bound in the error norm in the following Lemma.

Lemma 5.1 *Let $H(t) = \sum_X h_X$ be a local Hamiltonian as in Theorem 2. Then there are constants $\upsilon, \mu > 0$ such that for any disjoint regions A, B, C, we have*

$$\left\| U_t^{H_{A\cup B}} \left(U_t^{H_n}\right)^\dagger U_t^{H_{n\cup C}} - U_t^{H_{A\cup B\cup C}} \right\| \leq O\left(e^{\upsilon t - \mu\, \mathrm{dist}(A,C)}\right) \sum_{X:bd(AB,C)} \|hX\| \tag{5.6}$$

where X : bd(AB, C) means that $X \subseteq A \cup B \cup C$ and $X \not\subseteq A \cup B$ and $X \not\subseteq C$

The first term in the RHS shows an explicit exponential dependency of the error norm on the quantity υ, which is the same as the Lieb-Robinson velocity v_{LR}. Thus, it is certainly desirable to find as low an upper bound to v_{LR} as possible, in order to minimize the approximation error. In terms of the amount of quantum logic gates used, the authors' approach, utilizing the Lieb-Robinson bounds to simplify circuits have a gate complexity of $O(nT \text{ polylog } (nT/\epsilon))$ that is significantly better than the previous estimates of say, $O\left(n^2T \text{ polylog } (nT/\epsilon)\right)$ gates [13], or from Lie-Suzuki-Trotter expansions that have cost of $\left(n^2T(nT/\epsilon)^6\right)$ [4] gates.

Part III.

Methods And Techniques

6. Numerical Methods for Hyperbolic PDEs

6.1. Approaches

Numerical schemes for simulating PDEs are quite challenging in general. Not every method is created equal and each method has its advantages and disadvantages regarding accuracy, runtime, stability and storage requirements. There are broad approaches to the numerical solution of PDEs, namely : **Finite Difference Methods (FDM)**, **Finite Volume Methods (FVM)** and **Finite Element Methods (FEM)**. The FDM approach is somewhat easier to set up and can be further divided into **Explicit Methods** and **Implicit Methods**.

Explicit Methods

These methods involve setting up the numerical schemes in such a way that the value of some quantity of interest at a point in future depends only on its past values. Mathematically, for some quantity Y

$$Y(t + \Delta t) = F(Y(t)) \tag{6.1}$$

- Advantages : Fast, less storage required, no need to use expensive solvers to solve a system of equations.
- Disadvantages : Each method requires careful stability analysis and strict bounds on time-step size and spatial resolution. In other words, they are **Conditionally Stable**.

Implicit Methods

These methods involve setting up the numerical schemes in such a way that the value of some quantity of interest at a point in future depends not only on its past values, but also on its current value. This typically involves setting up a (possibly) non-linear system of equations and solving them to arrive at a solution. Mathematically, for some quantity Y, one needs to solve an equation of the form:

$$G(Y(t), Y(t + \Delta t)) = 0 \tag{6.2}$$

to be able to calculate $Y(t + \Delta t)$.

- Advantages : They are **Unconditionally Stable**.

- Disadvantages : Expensive storage and computation requirements as a large, possibly non-linear system of equation needs to be solved at each step.

6.2. Lax-Wendroff Scheme

For our purposes, we intend to solve the **1D Linear Advection Equation** formulated in Equation 4.7, which is hyperbolic in nature. For equations of this type, the **Lax-Wendroff Scheme** is a widely used explicit method. To formulate this scheme, let us consider a schematic:

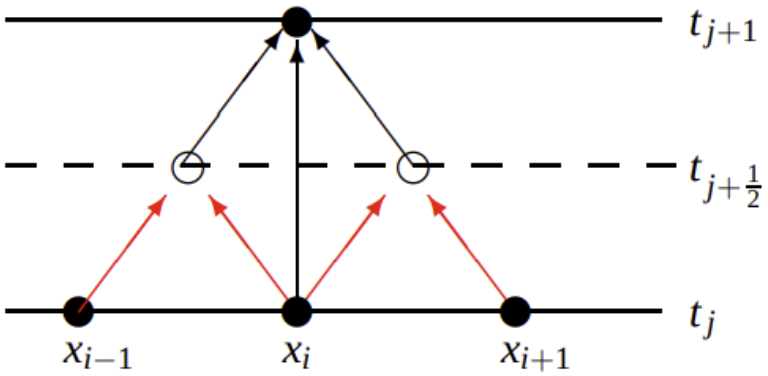

Figure 6.1.: Template for the Lax-Wendroff Scheme

Here, discrete time is shown on the vertical direction and discrete space is represented in the horizontal direction. In terms of nomenclature, an index on the superscript represents time and one on the subscript represents space. For example, x_i^{j+1} means the $i-$th point in space (along $x-$direction) at the $j-$th point in time. In this particular scheme, the index i always represents a spatial index and j always represents a temporal index.

The lax-Wendroff scheme is an example of a **multistep method** that uses data from multiple intermediate time-steps to calculate the value at the next time-step. Let us consider the Equation 4.7 again and calculate the value of quantity u at the point u_i^{j+1} using the intermediate half-steps. It looks like:

$$\begin{aligned} u_i^{j+\frac{1}{2}} &= u_i^j + \frac{\Delta t}{2}\left(-c\frac{\partial u}{\partial x}\bigg|_{(i,j)}\right) \\ u_i^{j+1} &= u_i^j + \Delta t\left(-c\frac{\partial u}{\partial x}\bigg|_{\left(i,j+\frac{1}{2}\right)}\right) \end{aligned} \tag{6.3}$$

Now we use the **central differences** to approximate the derivative $u_x|_{i,j+1/2}$ and we get:

$$u_i^{j+1} = u_i^j - \frac{c\Delta t}{\triangle x}\left(u_{i+\frac{1}{2}}^{j+\frac{1}{2}} - u_{i-\frac{1}{2}}^{j+\frac{1}{2}}\right) \tag{6.4}$$

On the second step the quantities $u_{i\pm\frac{1}{2}}^{j+\frac{1}{2}}$ can be calculated to obtain the following two-step scheme:

$$\begin{aligned} u_{i-\frac{1}{2}}^{j+\frac{1}{2}} &= \frac{1}{2}\left(u_i^j + u_{i-1}^j\right) - \frac{c\Delta t}{2\Delta x}\left(u_i^j - u_{i-1}^j\right) \\ u_{i+\frac{1}{2}}^{j+\frac{1}{2}} &= \frac{1}{2}\left(u_i^j + u_{i+1}^j\right) - \frac{c\Delta t}{2\Delta x}\left(u_{i+1}^j - u_i^j\right) \\ u_i^{j+1} &= u_i^j - \frac{c\Delta t}{\Delta x}\left(u_{i+\frac{1}{2}}^{j+\frac{1}{2}} - u_{i-\frac{1}{2}}^{j+\frac{1}{2}}\right) \end{aligned} \tag{6.5}$$

Equation 6.5 can be succinctly written as:

$$u_i^{j+1} = b_{-1}u_{i-1}^j + b_0 u_i^j + b_1 u_{i+1}^j, \tag{6.6}$$

with the constants being:

$$\begin{aligned} b_{-1} &= \frac{\alpha}{2}(\alpha+1) \\ b_0 &= 1-\alpha^2 \\ b_1 &= \frac{\alpha}{2}(\alpha-1) \end{aligned} \tag{6.7}$$

and $\alpha = \frac{c\Delta t}{\Delta x}$ is called the **Courant Number**. From the discretization, it can be seen that this method is second-order accurate in both time and space i.e $O(\Delta x^2, \Delta t^2)$.

6.3. Error Analysis

The Lax-Wendroff scheme being an explicit scheme, has to undergo error analysis in order to put bounds on the spatial and temporal resolutions so that a stable and physically correct simulation can be performed. The standard technique involves the **Von Neumann Stability Analysis** that involves the **Fourier Decomposition** of the quantity u at a particular time-step j into its **eigenmodes**, namely:

$$\mathbf{u}^j = (\xi)^j \tilde{\mathbf{u}} \tag{6.8}$$

This decomposition assumes the time independence of the eigenmodes. The coefficient ξ^j

is called the **Amplification factor** is is required to be less than one, for stable solutions. Using the approach mentioned in [8] and B.1, one arrives at the relation:

$$|\xi|^2 = 1 - \alpha^2 \left(1 - \alpha^2\right) \left(1 - \cos(k\Delta x)\right)^2 \tag{6.9}$$

As we require $|\xi|^2 \leq 1$, we obtain the relation:

$$\alpha = \frac{c\Delta x}{\Delta t} \leq 1 \tag{6.10}$$

This is called the **Courant-Friedrichs-Lewy Criterion** and it has to maintained during the numerical simulation.

6.4. Python Implementation

For implementing the Lax-Wendroff Scheme for the advection equation, the Python library **NumPy** is used for efficient array-based computations and the library **Matplotlib** is used for plotting solutions. The entire code is available in the file ***lax_wendroff.py***. The pseudocode is presented below, using the 0-based indexing that is used in Python.

Algorithm 1 Lax-Wendroff Scheme

Require: u_{old} : ndarray, $v > 0$: float, Δx : float, Δt : float.
Ensure: $\frac{v\Delta t}{\Delta x} \leq 1$

$c_1 \leftarrow \frac{v\Delta t}{2\Delta x}$
$c_2 \leftarrow 2c_1^2$
$N \leftarrow length(u_{old})$
$u_{new} \leftarrow u_{old}$

for $i : 0 \rightarrow (N-1)$ **do**
  if i is 0 **then**
    $u_{new}[0] \leftarrow u_{old}[0] - c_1 * (u_{old}[1] - u_{old}[-1]) + c_2 * (u_{old}[1] - 2 * u_{old}[0] + u_{old}[-1])$
  else if i is N-1 **then**
    $u_{new}[-1] \leftarrow u_{old}[-1] - c_1 * (u_{old}[0] - u_{old}[-1]) + c_2 * (u_{old}[0] - 2 * u_{old}[-1] + u_{old}[-2])$
  else
    $u_{new}[i] \leftarrow u_{old}[i] - c_1 * (u_{old}[i+1] - u_{old}[i-1]) + c_2 * (u_{old}[i+1] - 2 * u_{old}[i] + u_{old}[i-1])$
  end if
end for

return u_{new}

7. Numerical Estimation of Time Ordered Dynamical Correlations

7.1. Formulating the Hamiltonian

The first step in any quantum simulation is to set up the system in question and make some sanity checks as to its correctness. For our purpose, the exact state of the system, the **Quantum Wave Function** is not the most important part, as in, our experiments don't depend on a specific state or need to exclude some other ones. The Lieb-Robinson formulation [20] and the properties discussed in its context only depend on the Hamiltonian and the perturbations that are applied to the system. The interactions eventually affect the system itself, during the time-evolution, but the quantities that we estimate do not need an explicit description of the system state as long as it is a valid quantum state.

The formulation of the Hamiltonian is much more crucial for our purpose and care has to be taken to incorporate the correct boundary conditions which could be **Periodic** or **Open**. Open boundary conditions simulate a system where the system extends infinitely in all directions without any clear periodic structure. For a 1D case, it is analogous to a line segment extending infinitely in both directions. Periodic boundary conditions impose the notion of periodicity to the system in question by repeating the system structure repeatedly, beyond the system boundaries. For a 1D case, it can be thought of either as repeating a small line-segment over and over along a line or, as connecting the two ends of the line-segment to form a 'ring'. For our purposes, we use periodic boundary conditions.

The Hamiltonian is set up using an **Adjacency Matrix**, which is a convenient way of specifying the connectivity within a graph. Since a lattice can be though of as a graph, with the lattice sites being the **Nodes** and the connectivity between the nodes being the **Edges**. Large lattice sizes are difficult to simulate as the computation and space requirements grow exponentially with the number of lattice sites. The complete Hamiltonian for a lattice consisting of N sites is of the size 2^N x 2^N, with each entry being of the *complex* data type, that occupies 32 bytes in Python, compared to 24 bytes for a *Float16*. The growth of space requirements is shown in Figure 7.1:

Owing to the limited RAM on the computer used for simulations, the system size had to be confine to N = 13. However, this just takes care of the storage requirements and one still has to consider computational aspects from a **FLOP** or **Floating Point Operations**

perspective. In our simulation methods, matrix vector multiplications, tensor product operations and matrix exponential are essential and these are some of the most demanding operations in linear algebra from a FLOP perspective and they scale very poorly with system sizes. To alleviate this, we exploit the special nature of the Hamiltonian in question, namely, its **Sparsity**. Although the full Hamiltonian has 2^N x 2^N entries, most of the entries are zero and only a fraction of them are non-zero. The exact fraction depends on the Hamiltonian itself and the kind of interactions that are being modelled but for our case, the sparsity pattern is shown in Figure 7.2:

For a system with 13 lattice sites, and the full Ising Hamiltonian, only about 0.17% of the total entries are non-zero. To exploit this, we use the **Sparse Matrix** routines available in Python's **scipy.sparse** library to create the Hamiltonian.

The code for formulating the Hamiltonian was adapted from a Julia example, from [2] and is available in the file **hamiltonian.py**. The algorithm is outlined as follows:

Algorithm 2 Ising Hamiltonian

Require: J : float, h : float, $Adjacency\_Matrix$: matrix (NxN)

Ensure: $N \neq 0$

$X \leftarrow Pauli - X(\sigma^x_{2x2})$
$Z \leftarrow Pauli - Z(\sigma^z_{2x2})$
$L \leftarrow Adjacency\_Matrix.shape[0]$
$H \leftarrow scipy.sparse.csr\_matrix((2^L, 2^L), dtype = float)$

for $i : 0 \rightarrow (L-1)$ **do**
  for $j : (i+1) \rightarrow (L-1)$ **do**
    if Adjacency_Matrix[i,j] is 1 **then**
      $H- = J * (I_{2^i} \otimes (Z \otimes (I_{2^{j-i-1}} \otimes (Z \otimes I_{2^{L-j-1}}))))$
    end if
  end for
end for

for $i : 0 \rightarrow (L-1)$ **do**
  $H- = h * (I_{2^i} \otimes (X \otimes I_{2^{L-i-1}}))$
end for

return H

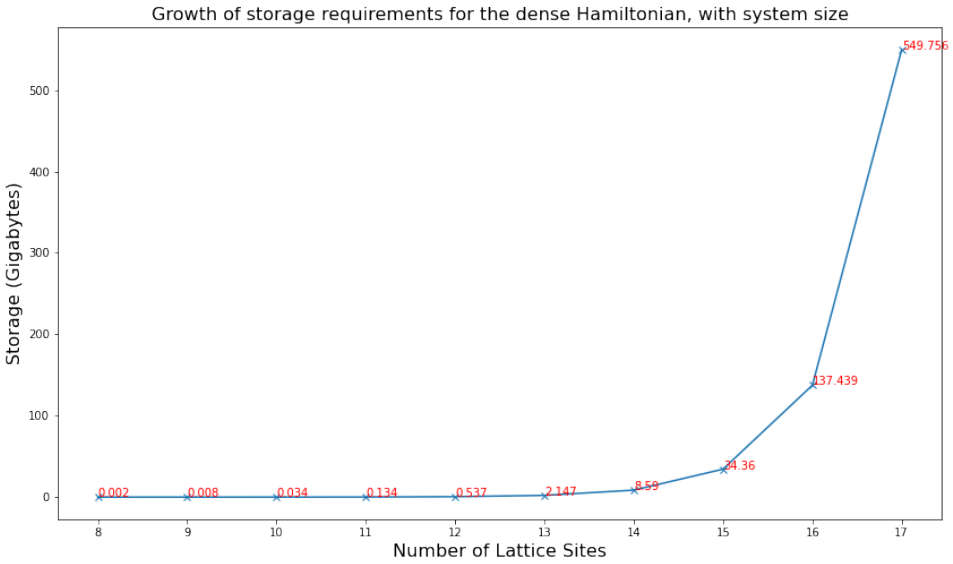

Figure 7.1.: Growth of storage requirements for the Hamiltonian, with the system size.

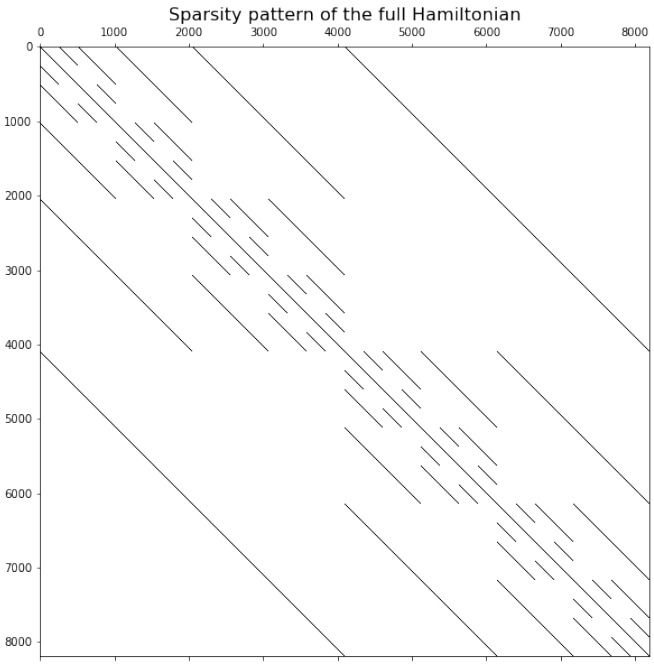

Figure 7.2.: Sparsity matrix.

7.2. Time Ordered Correlation Function

The correlation function follows the logic laid out in Equation 5.1 and is implemented in the file **correlation_function.py**. Aside from general inputs such as lattice size and the Hamiltonian, the most important parameters to calculate the correlations are the **site_operator**, which specifies the kind of perturbation that is applied at the given site (lattice-centre) at the start of our simulation. This corresponds to the operator V in Equation 5.1. In our case, the operator W is the same as V, except that it represents the time-evolved operator after time t. So we are effectively calculating the correlation between the operator $V(0)$ and $V(t)$ for different points in time. As mentioned before, we use sparse matrix operations to reduce the exponentially growing computation and storage requirements.

The most expensive step in our algorithm is the creation of a matrix exponential to obtain the unitary operator U from the Hamiltonian H, using the relation $U = e^{-iHt}$ and its subsequent multiplication with a quantum state to evolve it as $|\psi(t)\rangle = e^{-iHt}|\psi(0)\rangle$. This is quite challenging in general due to the fact that the matrix exponential for a sparse matrix is usually dense and then once again we are affected by the problems of dense formulations. There exist a certain class of methods, called **Krylov Subspace Methods** that circumvent this problem by never actually creating a full matrix-exponential by instead approximating the quantity $e^A X$ in an iterative fashion using some variants of algorithms such as the Lanczos Algorithm or the Conjugate Gradient Method [1]. This idea is neatly packaged into the SciPy's sparse routine **scipy.sparse.linalg.expm_multiply()**. This routine has unconditional stability in terms of the forward and backward error, for Hermitian matrices[1].

The algorithm to compute the correlation is as follows:

Algorithm 3 Time Ordered Correlation Function

Require: $lattice\_size$: int, $step\_size$: float, num_steps : int, $|\psi_0\rangle$: complex_array, $site\_operator$: complex_matrix, $hamiltonian$: complex_matrix.

Ensure: $step\_size \neq 0$, $num\_steps \neq 0$

$correlation\_data \leftarrow np.zeros((num\_steps, lattice\_size), dtype = "complex\_")$
$j \leftarrow lattice\_size/2$
$\sigma_j \leftarrow (I_{2^j} \otimes (site\_operator \otimes I_{2^{lattice\_size-j-1}}))$
$|\psi_{intermediate}\rangle \leftarrow \sigma_j \psi$

for $step : 0 \rightarrow (num\_steps - 1)$ **do**

  for $i : 0 \rightarrow (lattice\_size - 1)$ **do**
    $\sigma_i = (I_{2^i} \otimes (site\_operator \otimes I_{2^{lattice\_size-i-1}}))$
    $correlation\_data[step, i] = \langle\psi|\sigma_i|\psi_{intermediate}\rangle$
  end for

  $|\psi\rangle = e^{-(i*hamiltonian*step\_size)}|\psi\rangle$
  $|\psi_{intermediate}\rangle = e^{-(i*hamiltonian*step\_size)}|\psi_{intermediate}\rangle$

end for

return $correlation\_data$

8. Numerical Estimation of Lieb-Robinson Velocity

8.1. Numerical Estimate

Once the correlation data has been obtained from the method in **correlation.py**, we use a heurestic way of determining the Lieb-Robinson velocity. We simply keep track of the time at which the extreme site in the lattice first shows a correlation above a pre-defined threshold. If that time is t and if we assume the distance to the extreme lattice site to be d units, then the Lieb-Robinson velocity v_{LR} can be calculated as:

$$v_{LR} = \frac{d}{t} \quad = \frac{L/2}{n * dt} \tag{8.1}$$

where we have assumed that the distance between neighboring lattice sites is 1 unit, the initial perturbation is applied to the site at the middle of the chain and that the correlation at the extreme site reaches the minimum threshold after n iterations, each of duration dt. This calculation, along with some plotting tasks, are implemented in the file **lr_velocity.py**

8.2. Theoretical Estimate - Wang et al.

In order to compare the results from our numerical simulation, analytical bound on the v_{LR} from Wang and Hazzard [26] is used as reference. There are other works dealing with such bounds, such as Hastings Koma [15] and Nachtergaele [22] but the our reference stands out in its approach because the authors exploit the actual structure of the interactions to estimate an upper bound for unequal time commutators of local operators. This results in the tightest bounds for the v_{LR} till date, especially for translation-invariant, locally interacting systems such as the Ising Model. Their approach, especially within the context of the Ising Model, is as follows:

- **Step 1** : We first rewrite the hamiltonian H as $\hat{H} = \sum_j h_j \hat{\gamma}_j$, where $\hat{\gamma}_j$ represents the local operator, such as σ_i^x or $\sigma_i^x \sigma_j^x$ and the h_j are the coefficients, like J or h. From this we draw a **Commutativity Graph**, where each $\hat{\gamma}_j$ is represented by a vertex i and is joined to another vertex j only if the corresponding terms do not commute, i.e $[\hat{\gamma}_i, \hat{\gamma}_j] \neq 0$. For a 1D Ising Model, it may look something like this:

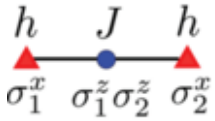

Figure 8.1.: Commutativity graph for $H = J\hat{\sigma}_1^z\hat{\sigma}_2^z + h\left(\hat{\sigma}_1^x + \hat{\sigma}_2^x\right)$. Courtesy : [26]

- **Step 2** : Next, we consider the Heisenberg evolution of an operator $\hat{\gamma}_j$ and formulate it time-evolution as follows:

$$i\dot{\hat{\gamma}}_i(t) = \left[\hat{\gamma}_i(t), \hat{H}\right] = \sum_{j:\langle ij\rangle\in G} h_j\left[\hat{\gamma}_i(t), \hat{\gamma}_j(t)\right] \tag{8.2}$$

  where the summation is performed only using the vertices j connected to the operator $\hat{\gamma}_j$. This enforces locality. The aim is to now find an upper bound to the unequal time-commutator $[\hat{A}(t), \hat{B}(0)]$ of two local operators $\hat{A}$ and $\hat{B}$.

- **Step 3** : The authors solve Equation 8.2 to obtain a general upper bound on $\hat{A}^B(t) = [\hat{A}(t), \hat{B}(0)]$ as:

$$\left\|\hat{A}^B(t)\right\| - \left\|\hat{A}^B(0)\right\| \leq \int_0^t \sum_{i\in S(\hat{A})} 2\|\hat{A}\|\,|h_i|\,\bar{\gamma}_i^B\left(t'\right)dt' \tag{8.3}$$

  where $S(\hat{A})$ represents the support of the operator $\hat{A}$ on the commutativity graph. Using an operator $\hat{\gamma}_i$ that appears in the Hamiltonian as $\hat{A}$ and the perturbation operator as $\hat{B}$, the general expression for v_{LR} is obtained as:

$$\left\|\left[\hat{\gamma}_i(t), \hat{B}_Y(0)\right]\right\| \leq \sum_{j\in Y} G_{ij}(t)\sqrt{\frac{h_j}{h_i}}2\|\hat{B}\| \tag{8.4}$$

  where, $G_{ij}(t)$ represent the Green's Function, used in solving the differential equations and $Y = S(\hat{B})$ represents the support of the operator $\hat{B}$ on the commutativity graph.

Using the general approach above, the authors have calculated the bound on the Lieb-Robinson for the TFIM as:

$$v_{\text{Ising}} \leq 2X_0\sqrt{dJh} \tag{8.5}$$

where $X_0 \approx 1.50888$ and d is the number of spatial dimensions in the lattice. Thus for a 1D TFIM, the expression reduces to:

$$v_{\text{Ising}} \leq 3.02\sqrt{Jh} \tag{8.6}$$

Part IV.

Results and Conclusion

9. Results

9.1. Linear Advection Equation

To start with, the classical Linear Advection Equation is simulated using the Algorithm 1. N=100 uniformly spaced grid-points are chosen inside the X-domain $x \in [0, 1]$. The spatial resolution Δx is set as $\Delta x = 1/N$ and the advection velocity v is set to 1.0 m/s. The temporal resolution is set inside the method by using the CFL condition. Since we derived in Equation 6.10 that the CFL number must be less than or equal to 1, we choose two test cases : one that adheres to this condition and one that violates it. The CFL numbers chosen are 0.8 and 1.005. The initial condition $u(x, 0)$ is set as:

$$u(x,0) = \begin{cases} 1.0, \text{ if } x \in (a,b) \\ 0.0, \text{ otherwise} \end{cases} \tag{9.1}$$

The domain (a, b) is selected in the program, based on the grid-size. The initial setup looks as follows:

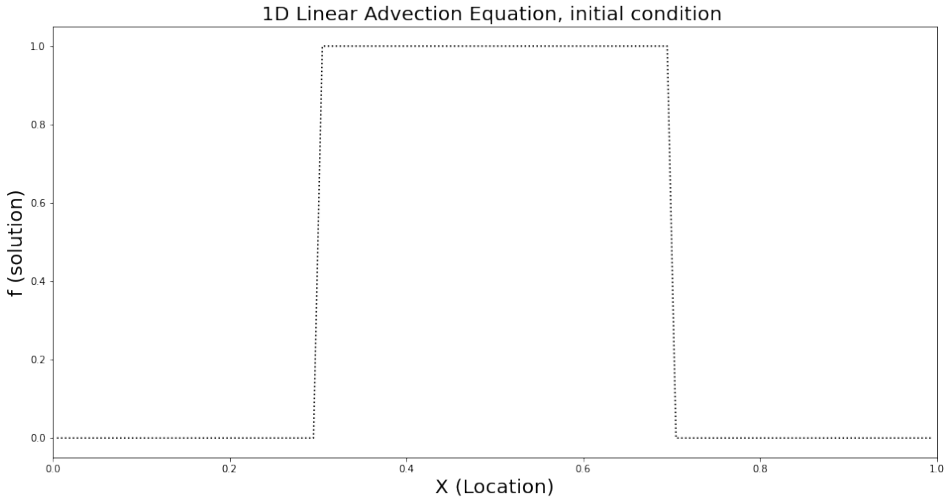

Figure 9.1.: Initial conditions for the Linear Advection Equation

The results of the finite-difference simulation is plotted in the following figure:

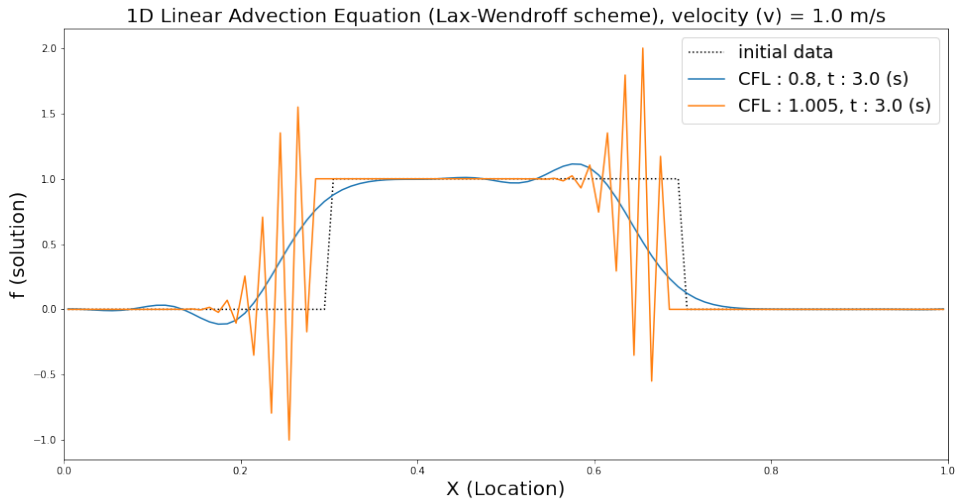

Figure 9.2.: Initial conditions for the Linear Advection Equation

It can be clearly seen that, when the CFL number exceeds 1, unwanted oscillations are introduced in the solution and it becomes unusable. When kept below 1, the solutions display physically correct behaviour, within the limits of error that is inherent to the discretization scheme being used.

9.2. Light Cones for Dynamical Correlations

The quantum simulations for the TFIM are run on a system with lattice size L**=13**, with N**=100** timesteps, each of step-size dt**=0.007** seconds. The initial state-vector $|\Psi_0\rangle$ is generated randomly and the perturbation operator, a $Pauli - X$ operator, is made to act at the centre of the lattice. The strength of the external field, h **is set to -0.5** and the value of J **is varied from -3 to 3**, in order to gather experimental data.

At every instance of the simulation, the light-cone boundaries predicted by both the simulations as well as the reference upper bound, is overlaid on top of the correlation data to see which method predicts a more accurate bound. The calculated velocities only depend on the magnitude of J and not the sign, so the graphs are nearly identical for the same value of J but with different signs.

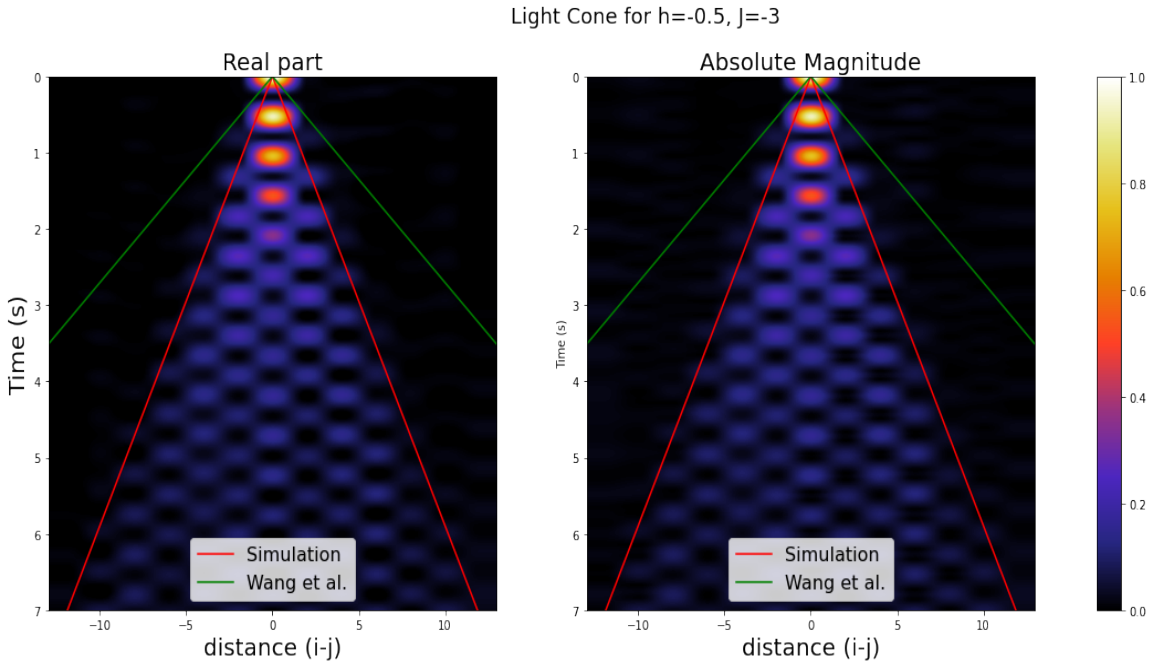
Light Cone for h=-0.5, J=-3
Real part
Absolute Magnitude
Time (s)
distance (i-j)
Simulation
Wang et al.

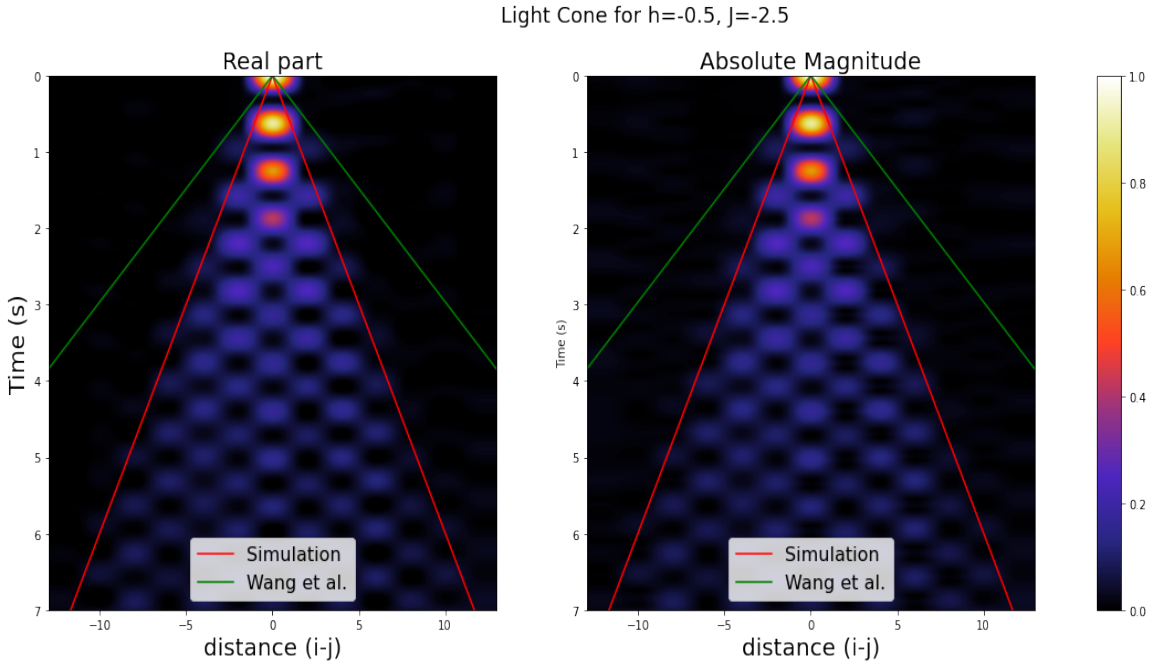
Light Cone for h=-0.5, J=-2.5
Real part
Absolute Magnitude
Time (s)
distance (i-j)
Simulation
Wang et al.

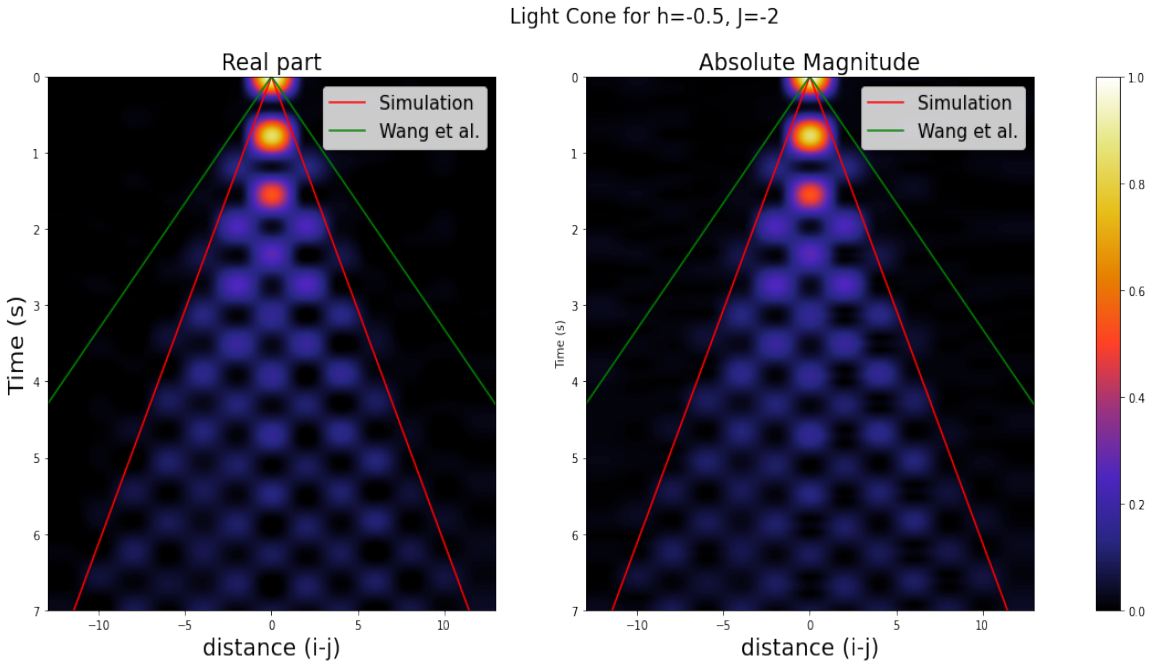
Light Cone for h=-0.5, J=-2
Real part
Absolute Magnitude
Simulation
Wang et al.
Time (s)
distance (i-j)

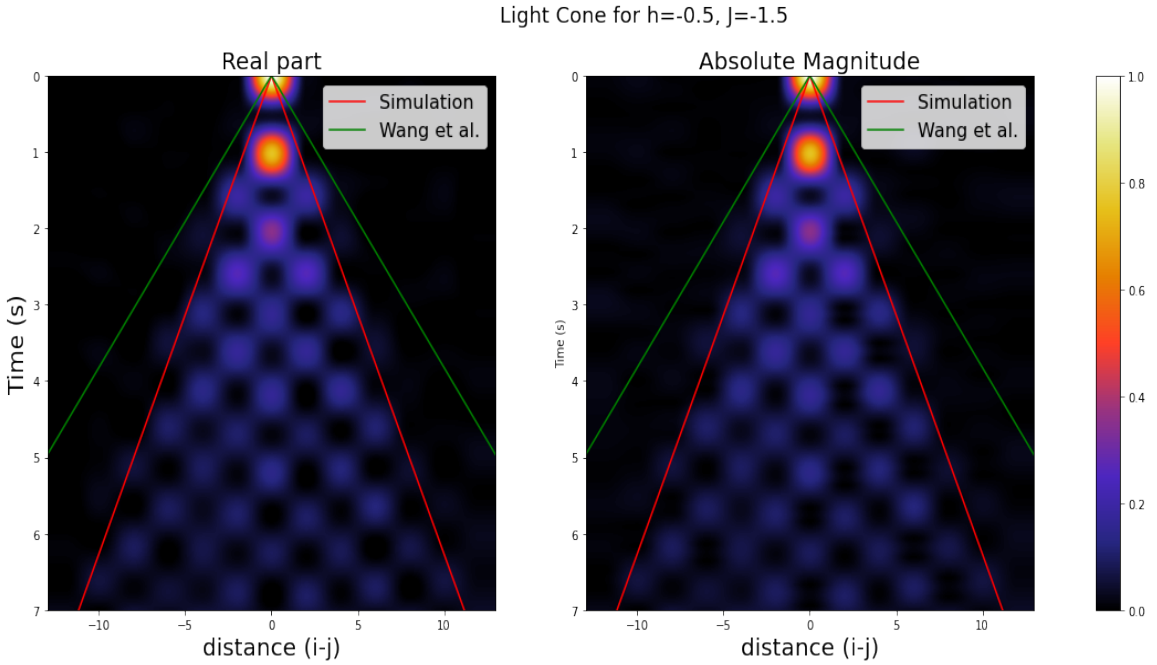
Light Cone for h=-0.5, J=-1.5
Real part
Absolute Magnitude
Simulation
Wang et al.
Time (s)
distance (i-j)

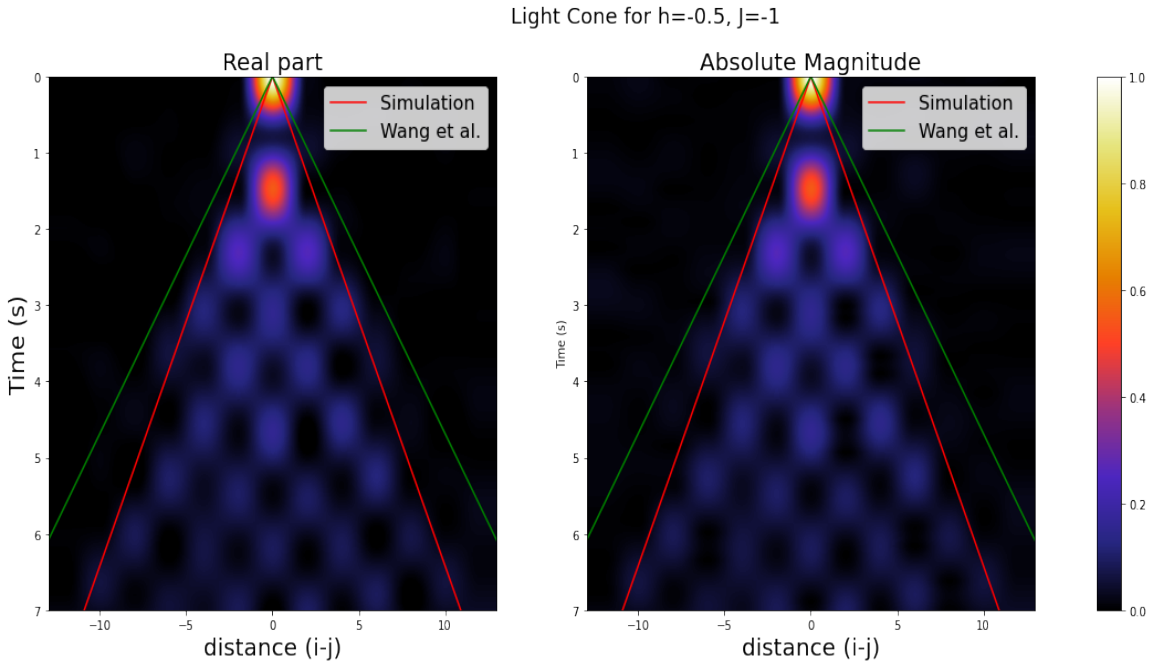
Light Cone for h=-0.5, J=-1
Real part
Absolute Magnitude
Simulation
Wang et al.
Time (s)
distance (i-j)

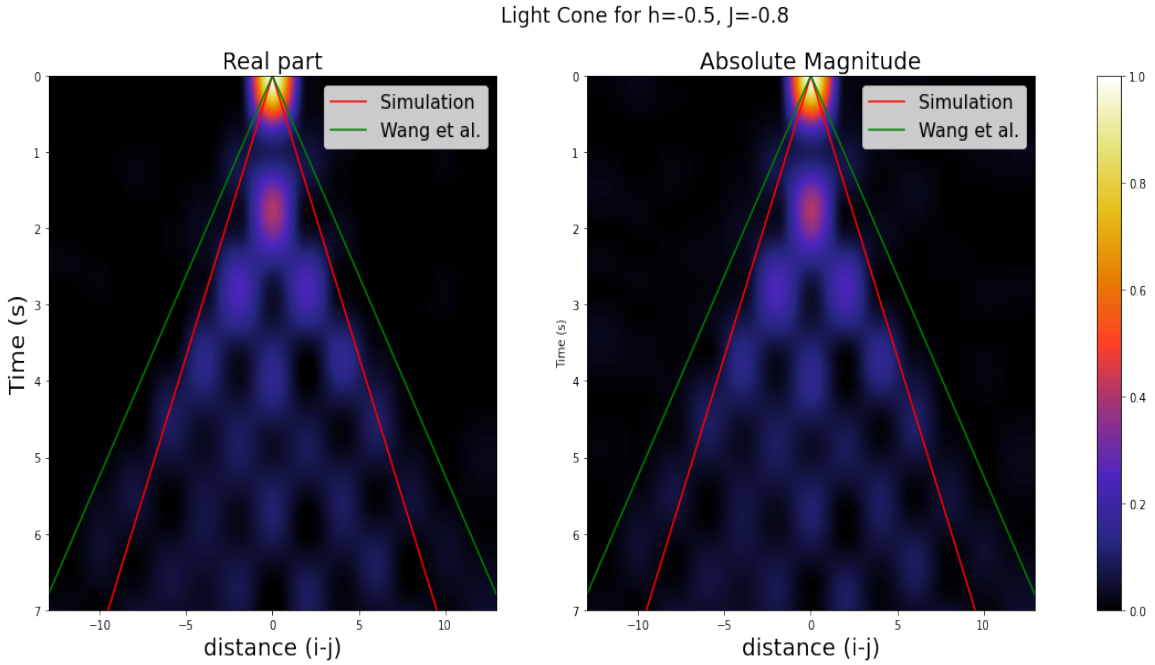
Light Cone for h=-0.5, J=-0.8
Real part
Absolute Magnitude
Simulation
Wang et al.
Time (s)
distance (i-j)

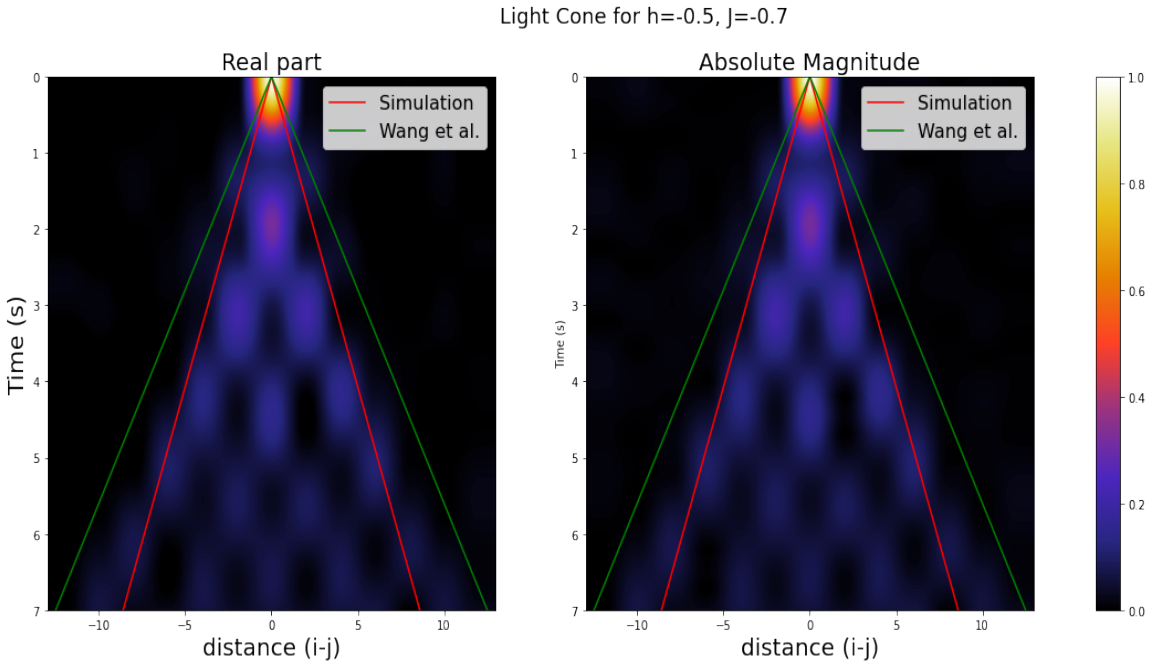
Light Cone for h=-0.5, J=-0.7
Real part
Absolute Magnitude
Simulation
Wang et al.
Time (s)
distance (i-j)

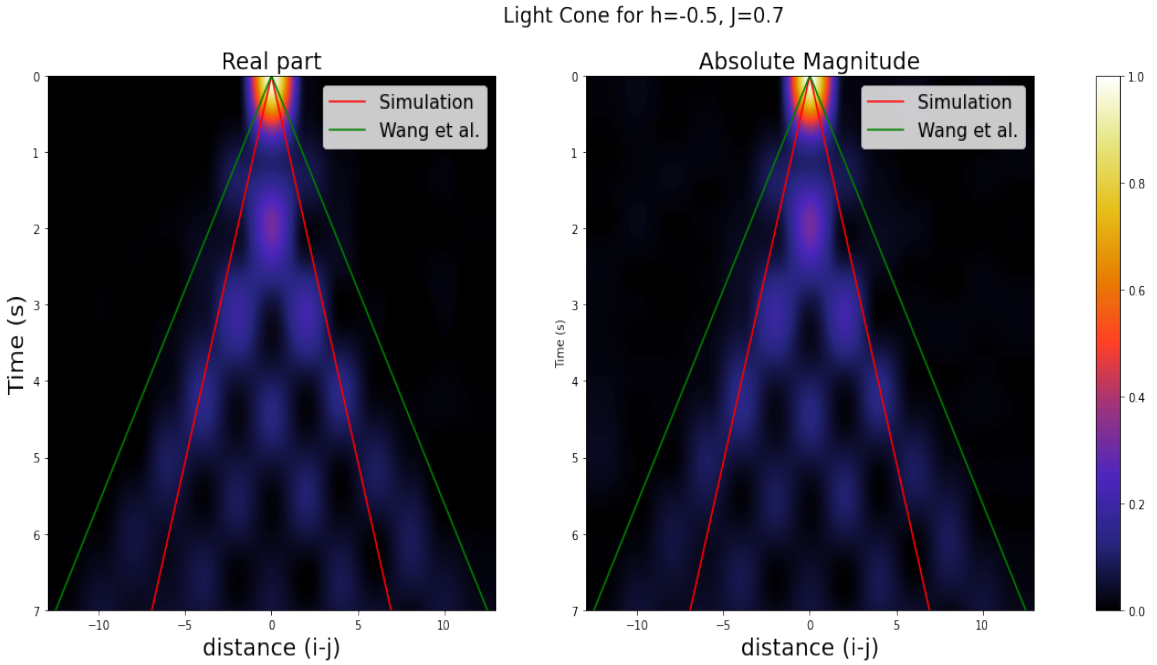
Light Cone for h=-0.5, J=0.7
Real part
Absolute Magnitude
Simulation
Wang et al.
Time (s)
distance (i-j)

Of interest is also the plot for the special case where J is set to 0, implying the total absence of correlations in the system. As expected, a light-cone is not seen in this case. In some plots, such as the one corresponding to $J = 0.7$, it can be seen that some correlation 'leaks' beyond the estimated light-cone. However, this should not be an issue since the v_{LR} is not meant to be a hard cut-off for the information spread but rather as a bound beyond which the information spread, quantified here by correlations, decay exponentially. All the plots adhere to this criterion.

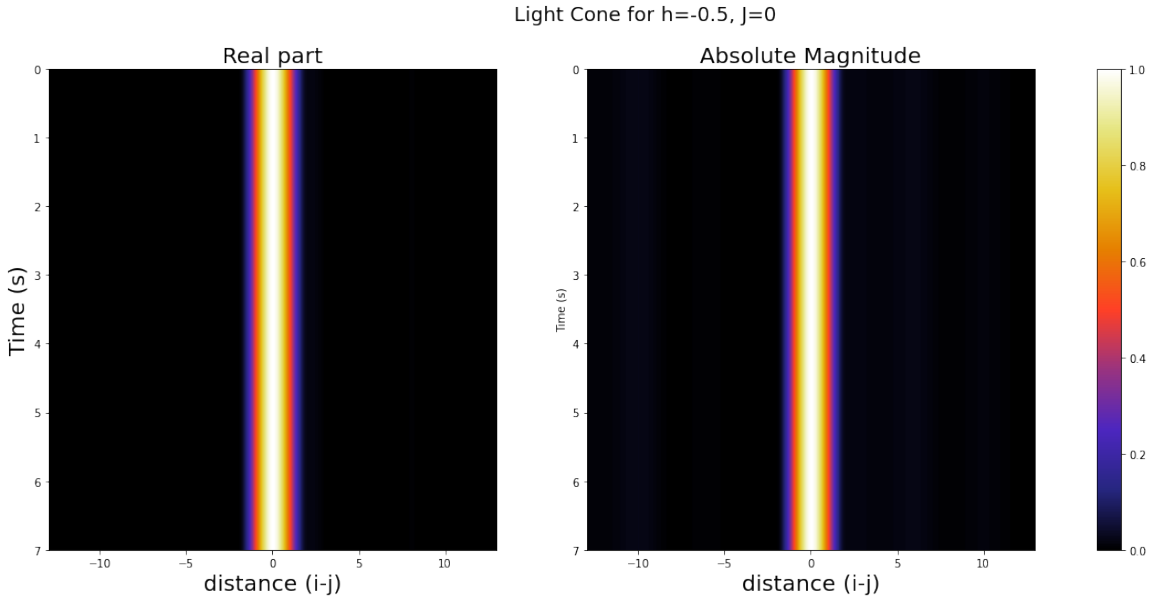

Figure 9.7.: Absence of a light-cone when J=0

A closer look is also taken on how the correlations actually evolve at the sites sites over time as well as how the correlations change at specific sites, in the following figure.

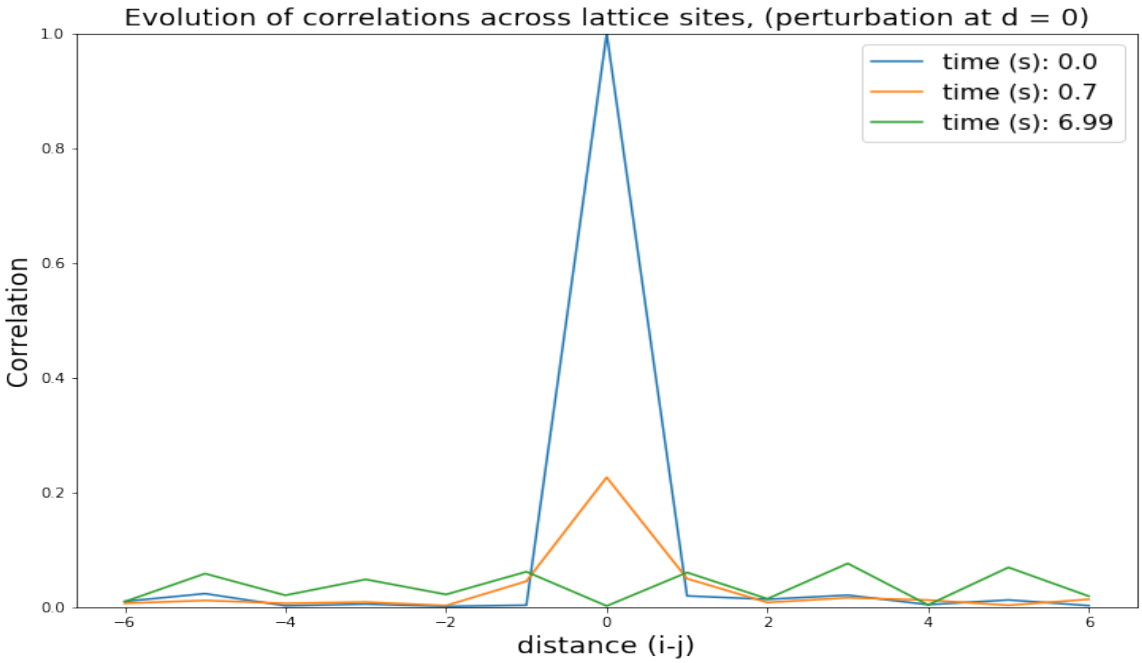
Evolution of correlations across lattice sites, (perturbation at d = 0)
time (s): 0.0
time (s): 0.7
time (s): 6.99
Correlation
distance (i-j)

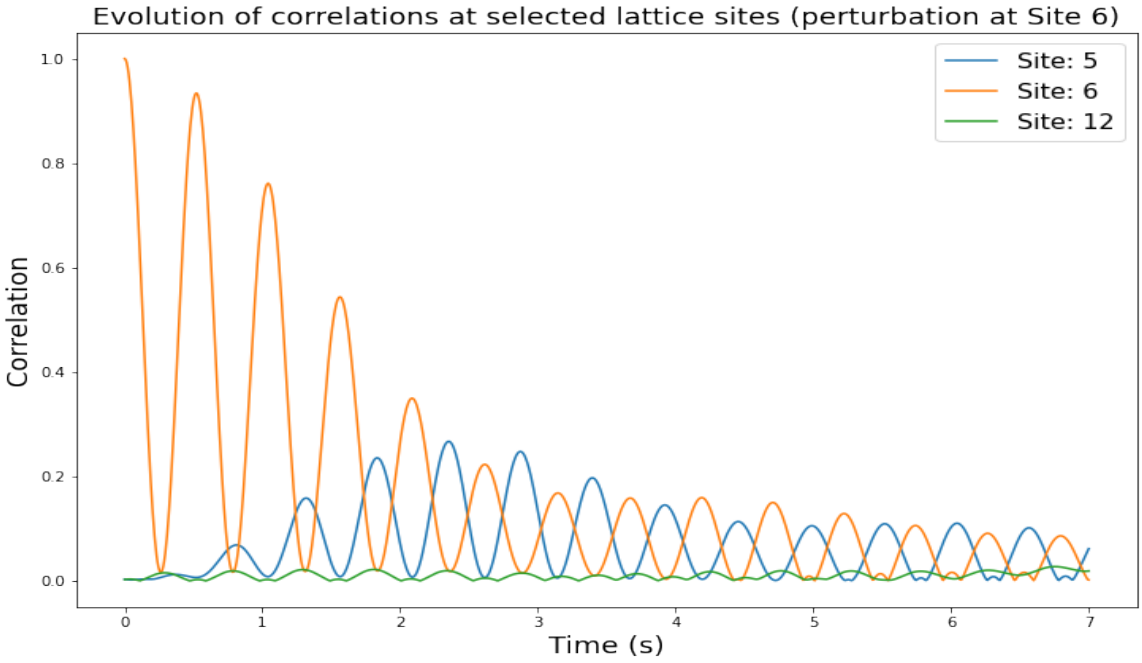
Evolution of correlations at selected lattice sites (perturbation at Site 6)
Site: 5
Site: 6
Site: 12
Correlation
Time (s)

9.3. Comparison between Theoretical and Numerical Approaches

Looking at the light-cone boundaries in the plots, it is seen that the reference analytical solution from Wang et al. provides a rather loose bound on the v_{LR}, especially at $|J| > 1$. However, the estimate from the numerical experiments provide a really tight bound that envelopes the complete light-cone and beyond the boundaries of the cone, the correlations decay rapidly to zero, as predicted by the theory. A comparison between the values from the simulation and from the reference is presented in Figures 9.9 and 9.11. In Figure 9.9, in addition to the numerical and reference values, an interpolation line based on the numerical results is also provided, that can be use to obtain the value of v_{LR} in this region.

The theory behind the Lieb-Robinson bounds [20], [26] predicts that the v_{LR} should not keep increasing as the value of $|J|$ rises but should ideally slow down with increasing $|J|$. This behaviour is observed from the simulations where the $|J|$ noticeably plateaus after $|J| > 1$. The estimate from [26] keep rising monotonically as in that particular formulation, $v_{LR} \propto \sqrt{|J|}$

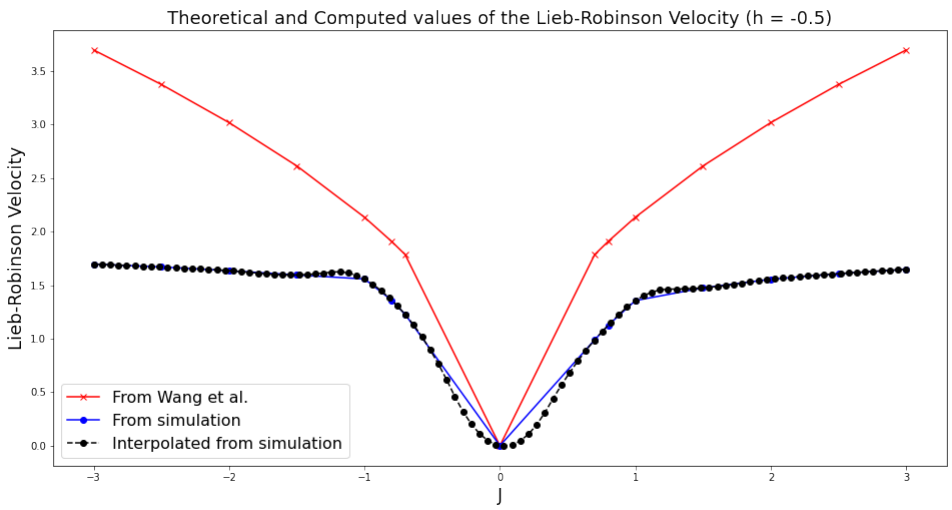

Figure 9.9.: Comparison of v_{LR} from simulation and reference

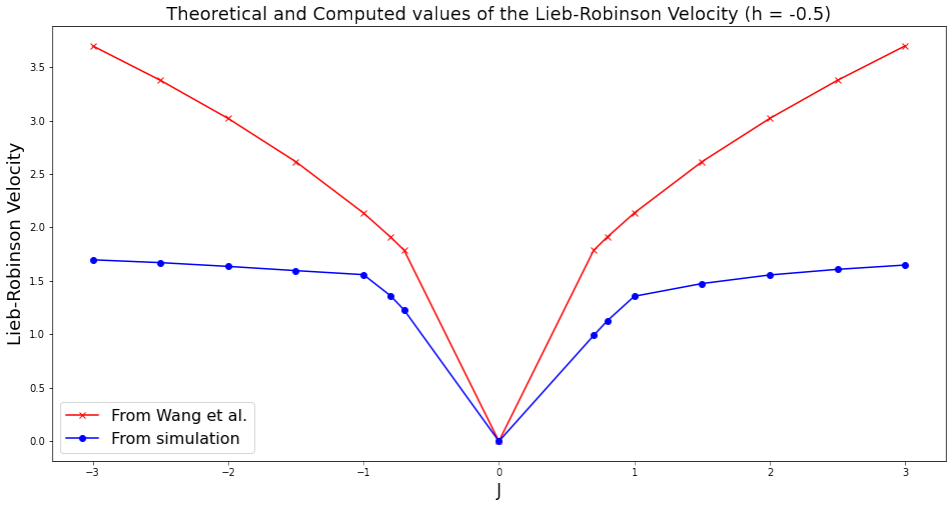

Figure 9.10.: Comparison of v_{LR} from simulation and reference

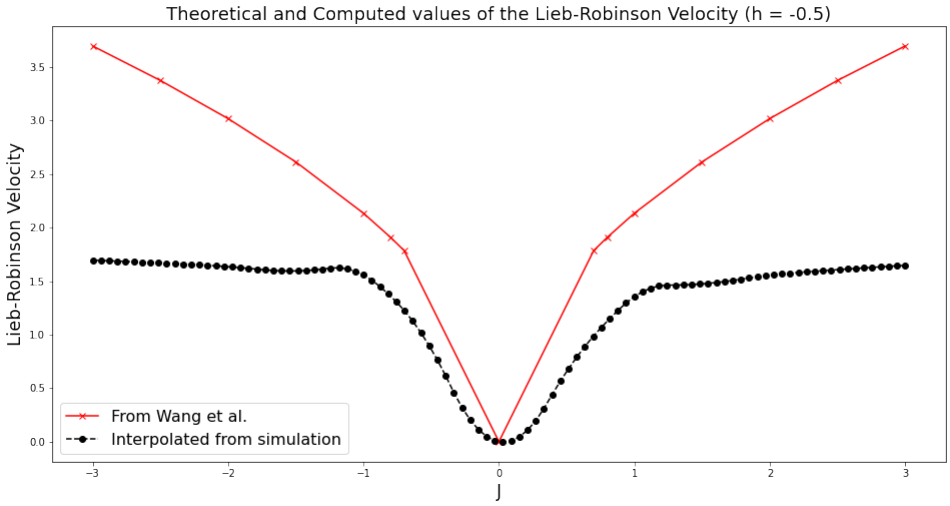

Figure 9.11.: Comparison of v_{LR} from interpolation and reference

10. Conclusions

10.1. General Conclusions

The code snippets used for simulation are all available in the repository : thesis-code. The classical simulation is performed inside the notebook **classical_simulation.ipynb** and the quantum simulation is performed inside the notebook **quantum_simulation.ipynb**

From the results obtained by using the time-ordered correlation functions to directly estimate the v_{LR}, it can be seen that in translation invariant quantum systems governed by local interactions, information indeed spreads at a finite speed and it takes a finite amount of time for one part of the system to get affected by perturbations in another part of the system, in close analogy with classical systems governed by wave-like dynamics. During the interval when distant parts of the system are not yet correlated to some extent, their time-evolution can be treated in an independent manner by considering the separate parts to be separate subsystems. As discussed before, this has important implications in quantum simulations on digital quantum computers. So a better estimate of the v_{LR} that does not overestimate it, holds the potential to divide a system into more independent subsystems and treat them so for longer time-steps, reducing computational requirements along the way. The ideas outlined in this thesis are certainly a viable path for estimating v_{LR} in systems that are not too large in size, or for systems that may be large but exhibit a periodic structure, such as crystals.

10.2. Improvement Areas and Future Work

The methods and techniques described in this thesis are strictly confined to Hamiltonians that are local in nature. The case for systems that have long-range interactions need to be incorporated to come up with a more general simulation framework to determine the speed at which information spreads in such systems. Also, it would be a worthwhile task to examine other Hamiltonians that are also local, such as the **Bose-Hubbard Model**, **Cluster Hamiltonians** etc and study how the v_{LR} is related to the system parameters in these cases.

11. List of Figures and Algorithms

List of Algorithms

List of Figures

Appendix

A. Postulates Of Quantum Mechanics

A.1. Postulates

While discussing quantum mechanics, one has to distinguish between two separate aspects, one being the **mathematical formalism** and the other being the **ontological status**. The ontological status, or the interpretation of the postulates and quantities of quantum mechanics, is an usolved problem and there are different schools of thought, often polar opposite to one another. However, the mathematical formulation of the laws that govern quantum mechanisc have been well established almost a century ago and are extremely consistent with experiments and observations obtained quantum phenomena. They are summarized under:

- **Postulate 1** : The state of a physical system at any instant is represented by a **ket** $|\psi\rangle$ in the space of states, that forms a **Hilbert Space** equipped with an **Inner Product**, $\langle , \rangle$
- **Postulate 2** : Every observable attribute of any physical system is described by an operator that acts on the ket that represents the system. An operator $\hat{\mathcal{A}}$ acting on a ket $|\psi\rangle$, is denoted as $\hat{\mathcal{A}} : |\psi\rangle \rightarrow |\psi'\rangle = \hat{\mathcal{A}}|\psi\rangle$
- **Postulate 3** : The possible result that can be observed after measuring an observable $\hat{\mathcal{A}}$ is one of the eigenvalues of the operator.
- **Postulate 4** : When an observable $\hat{\mathcal{A}}$ is measured on a generic state $|\psi\rangle$, the probability of obtaining an eigenvalue a_n is given by the square of the inner product of $|\psi\rangle$ with the eigenstate $|n\rangle : |\langle a_n \mid \psi\rangle|^2$
- **Postulate 5** : Immediately after the measurement of the observable $\hat{\mathcal{A}}$ yields a value a_n, the state of the system becomes the normalized eigenstate $|n\rangle$.
- **Postulate 6** : The time-evolution of the state of a quantum system is described by a unitary operator $\hat{U}$ as : $|\psi(t)\rangle = U\left(t, t_0\right)|\psi\left(t_0\right)\rangle$.

B. Von-Neumann Stability Analysis

B.1. Proof

While establishing the stability criterion of the Lax-Wendroff scheme, we examine the solution at a particular point on the grid i at a time-step j and decompose it into its fourier modes. In Equation B.1, we wrote it as:

$$\mathbf{u}^j = (\xi)^j \tilde{\mathbf{u}} \tag{B.1}$$

We choose a solution ansatz of the following form, which, at a given instant j only depends on spatial location i:

$$\mathbf{u}_i^j = (\xi)_i^j e^{Iik\Delta x} \tag{B.2}$$

where, k is the wave-number of the mode and $\xi = \xi(k)$ is the **Amplification Factor** and $I = \sqrt{-1}$ so as to not mix it up with i. Note that this is the expression for a single harmonic of the fourier series, the one with wave-number k. For a scheme to be stable:

$$\left| \frac{(\xi)_i^{j+1}}{(\xi)_i^j} \right| \leq 1 \tag{B.3}$$

The time derivative of the scheme is given by :

$$u\left(x_i, t_{j+1}\right) = u\left(x_i, t_j\right) - c\Delta t \partial_x u\left(x_i, t_j\right) + \frac{c^2 \Delta t^2}{2} \partial_x^2 u\left(x_i, t_j\right) + O\left(\triangle t^2\right) \tag{B.4}$$

using the central difference for space derivatives, and inserting the ansatz, we obtain:

$$\begin{aligned} \frac{u\left(x_i, t_{j+1}\right)}{u\left(x_i, t_j\right)} &= 1 - c\Delta t \frac{\mathrm{e}^{\mathrm{i}k\Delta x} - \mathrm{e}^{-\mathrm{i}k\Delta x}}{2\Delta x} + \frac{c^2 \Delta t^2}{2} \frac{\mathrm{e}^{\mathrm{i}k\Delta x} - 2 + \mathrm{e}^{-\mathrm{i}k\Delta x}}{\Delta x^2} \\ &= 1 - \mathrm{i}\alpha \sin(k\Delta x) + \alpha^2(\cos(k\Delta x) - 1) \end{aligned} \tag{B.5}$$

where $\alpha = c\frac{\Delta t}{\Delta x}$ is the Courant number. Calculating the squared modulus of B.5, we have:

$$\begin{aligned} |\xi|^2 &= \left(1 - \alpha^2(1 - \cos(k\Delta x))\right)^2 + \alpha^2\left(1 - \cos^2(k\Delta x)\right) \\ &= 1 - 2\alpha^2(1 - \cos(k\Delta x)) + \alpha^2\left(1 - \cos^2(k\Delta x)\right) + \alpha^4(1 - \cos(k\Delta x))^2 \\ &= 1 - \alpha^2\left(1 - \alpha^2\right)(1 - \cos(k\Delta x))^2 \\ &= 1 - 4\alpha^2\left(1 - \alpha^2\right)\sin^4\left(\frac{1}{2}k\Delta x\right). \end{aligned} \tag{B.6}$$

For the scheme to be stable according to the von Neumann criterion, $|\xi|^2 \leq 1$, and this gives $\alpha \leq 1$.

Bibliography

[1] Computing the action of the matrix exponential, with an application to exponential integrators. http://eprints.ma.man.ac.uk/1591/. Accessed: 2021-09-30.

[2] Qaintessent : Hamiltonian from adjacency matrix. https://github.com/Qaintum/Qaintellect.jl. Accessed: 2021-09-30.

[3] F. Barratt, James Dborin, Matthias Bal, Vid Stojevic, Frank Pollmann, and A. G. Green. Parallel quantum simulation of large systems on small nisq computers. *npj Quantum Information*, 7(1), May 2021.

[4] Dominic W. Berry, Graeme Ahokas, Richard Cleve, and Barry C. Sanders. Efficient quantum algorithms for simulating sparse hamiltonians. *Communications in Mathematical Physics*, 270(2):359–371, dec 2006.

[5] Jacob Biamonte and Ville Bergholm. Tensor networks in a nutshell, 2017.

[6] A Bohrdt, C B Mendl, M Endres, and M Knap. Scrambling and thermalization in a diffusive quantum many-body system. *New Journal of Physics*, 19(6):063001, jun 2017.

[7] A Bohrdt, C B Mendl, M Endres, and M Knap. Scrambling and thermalization in a diffusive quantum many-body system. *New Journal of Physics*, 19(6):063001, jun 2017.

[8] J. G. Charney, R. FjÖrtoft, and J. Von Neumann. Numerical integration of the barotropic vorticity equation. *Tellus*, 2(4):237–254, 1950.

[9] R Courant, K Friedrichs, and H Lewy. *Mathematische Annalen*. 1928.

[10] A. Einstein, B. Podolsky, and N. Rosen. Can Quantum-Mechanical Description of Physical Reality Be Considered Complete? *Physical Review*, 47(10):777–780, May 1935.

[11] Alexander L Fetter and John Dirk Walecka. *Quantum theory of many-particle systems*. Courier Corporation, 2012.

[12] Martin Gebert, Alvin Moon, and Bruno Nachtergaele. A lieb-robinson bound for quantum spin chains with strong on-site impurities. 2021.

[13] Hrant Gharibyan, Masanori Hanada, Masazumi Honda, and Junyu Liu. Toward simulating superstring/m-theory on a quantum computer. *Journal of High Energy Physics*, 2021(7), jul 2021.

[14] Jeongwan Haah, Matthew Hastings, Robin Kothari, and Guang Hao Low. Quantum algorithm for simulating real time evolution of lattice hamiltonians. In *2018 IEEE 59th Annual Symposium on Foundations of Computer Science (FOCS)*, pages 350–360, 2018.

[15] Matthew B. Hastings and Tohru Koma. Spectral gap and exponential decay of correlations. *Communications in Mathematical Physics*, 265(3):781–804, apr 2006.

[16] Farzan Jazaeri, Arnout Beckers, Armin Tajalli, and Jean-Michel Sallese. A review on quantum computing: Qubits, cryogenic electronics and cryogenic mosfet physics. 2019.

[17] B. Kraus and J. I. Cirac. Optimal creation of entanglement using a two-qubit gate. *Physical Review A*, 63(6), May 2001.

[18] Tomotaka Kuwahara and Keiji Saito. Lieb-robinson bound and almost-linear light cone in interacting boson systems. *Physical Review Letters*, 127(7), Aug 2021.

[19] Peter Lax and Burton Wendroff. Systems of conservation laws. *Communications on Pure and Applied Mathematics*, 13(2):217–237, 1960.

[20] Elliott H. Lieb and Derek W. Robinson. The finite group velocity of quantum spin systems. *Communications in Mathematical Physics*, 28(3):251–257, September 1972.

[21] Sheng-Hsuan Lin, Rohit Dilip, Andrew G. Green, Adam Smith, and Frank Pollmann. Real- and imaginary-time evolution with compressed quantum circuits. *PRX Quantum*, 2(1), Mar 2021.

[22] Bruno Nachtergaele and Robert Sims. Lieb-robinson bounds and the exponential clustering theorem. *Communications in Mathematical Physics*, 265(1):119–130, mar 2006.

[23] Bruno Nachtergaele and Robert Sims. Lieb-robinson bounds in quantum many-body physics, 2010.

[24] Michael A. Nielsen and Isaac L. Chuang. *Quantum Computation and Quantum Information*. Cambridge University Press, 2000.

[25] Minh C. Tran, Andrew Y. Guo, Yuan Su, James R. Garrison, Zachary Eldredge, Michael Foss-Feig, Andrew M. Childs, and Alexey V. Gorshkov. Locality and digital quantum simulation of power-law interactions. *Phys. Rev. X*, 9:031006, Jul 2019.

[26] Zhiyuan Wang and Kaden R.A. Hazzard. Tightening the lieb-robinson bound in locally interacting systems. *PRX Quantum*, 1:010303, Sep 2020.